EUROPEAN LABORATORY FOR PARTICLE PHYSICS

CERN-SPSC/97–5
SPSC/I 213
March 14, 1997

LETTER OF INTENT

A HIGH SENSITIVITY SHORT BASELINE EXPERIMENT TO SEARCH FOR $\nu_\mu \to \nu_\tau$ OSCILLATION

A. S. Ayan, E. Pesen, M. Serin-Zeyrek, R. Sever, P. Tolun, M. T. Zeyrek:
METU, Ankara, Turkey

N. Armenise, F. Cassol, M. G. Catanesi, M. T. Muciaccia, E. Radicioni, S. Simone, L. Vivolo:
Università di Bari and INFN, Bari, Italy

A. Meyer-Sievers, K. Winter: **Humboldt Universität, Berlin, Germany**

D. Bertrand, M. Vander Donckt[1], B. Van de Vyver[2], P. Vilain[3], G. Wilquet[3]:
Inter-University Institute for High Energies (ULB-VUB), Brussels, Belgium

B. Saitta: **Università di Cagliari and INFN, Cagliari, Italy**

A. Bueno, G. Feldman, S. Mishra: **Harvard University, Cambridge , MA, USA**

C. Gössling, D. Pollmann, B. Lisowski: **Dortmund Universität, Dortmund, Germany**

S. Bunyatov, V. Kuznetsov, B. Popov, V. Tereshchenko: **JINR, Dubna, Russia**

E. Di Capua: **Università di Ferrara and INFN, Ferrara, Italy**

E. Iacopini, G. Graziani, A. Lupi: **Università di Firenze and INFN, Florence, Italy**

S. Ogawa, H. Shibuya: **Toho University, Funabashi, Japan**

J. Brunner, L. Camilleri, A. Cervera, D. Cussans, L. Di Lella, E. do Couto e Silva, J. P. Fabre, R. Ferreira[4], D. Ferrere, A. Geiser, J.J. Gomez-Cadenas, A. Grant, J.A. Hernando[5], M. de Jong, J. Kokkonen, L. Linssen, M. Litmaath, L. Ludovici[6], H. Meinhard, E. Niu, J. Panman, I. Papadopoulos, S. Ricciardi[7], O. Runolfsson, D. Saltzberg, E. Tsesmelis, F. Wilson, H.T. Wong[8], P. Zucchelli: **CERN, Geneva, Switzerland**

J. Goldberg: **Technion, Haifa, Israel**

S. Aoki, T. Hara: **Kobe University, Kobe, Japan**

M. Reyes-Rivet, D. Steele, M.T. Tran: **Université de Lausanne, Lausanne, Switzerland**

D. Favart, J. Govaerts, G. Grégoire:
Université Catholique de Louvain, Louvain-la-Neuve, Belgium

S. Tovey: **University of Melbourne, Melbourne, Australia**

S. Gninenko, A. Kovzelev, A. Toropin, S. Volkov: **Inst. Nucl. Research, INR Moscow, Russia**

D. Bonekämper, D. Frekers, D. Rondeshagen, H.J. Wörtche:
Münster Universität, Münster, Germany

K. Hoshino, K. Niwa: **Nagoya University, Nagoya, Japan**

S. Buontempo, A. G. Cocco, N. D'Ambrosio, A. Ereditato, G. Fiorillo, M. Messina, P. Migliozzi, V. Palladino, S. Sorrentino, P. Strolin: **Università Federico II and INFN, Naples, Italy**

M. Baldo-Ceolin, D. Gibin, A. Gugliemi, M. Laveder, M. Mezzetto:
Università di Padova and INFN, Padova, Italy

A. Capone, U. Dore, P. F. Loverre, G. Piredda, G. Rosa, R. Santacesaria:
Università La Sapienza and INFN, Rome, Italy

G. Bozza, A. di Bartolomeo, G. Grella, G. Iovane, G. Romano:
Università di Salerno and INFN, Salerno, Italy

L. Peak, P. Soler, K. Varvell: **University of Sydney, Sydney, Australia**

The following institutes expressed their interest:
ITEP (Moscow), **NIKHEF** (Amsterdam), **Saclay**
and are participating in R&D projects.

[1]Fonds pour la Formation a la Recherche dans l'Industrie et dans l'Agriculture
[2]National Fonds voor Wetenschappelijk Onderzoek
[3]Fonds National de la Recherche Scientifique
[4]Supported by JNICT - Junta Nacional de Investigação, Científica e Tecnológica, PROGRAM PRAXIS XXI.
[5]Permanent adress: University of Valencia, Valencia, Spain.
[6]On leave of absence from Università 'La Sapienza' and INFN, Rome, Italy
[7]supported by Fondazione Angelo Della Riccia
[8]Leave of Absence at the Academia Sinica, Taiwan

1 Introduction

One of the most interesting open questions in particle physics is the possibility that neutrinos have non-vanishing masses and, therefore, that oscillations among the different families may occur. Massive neutrinos are natural candidates for the hot component of the dark matter of the universe [1]. Neutrino oscillation has been long considered a likely explanation of the solar neutrino deficit [2, 3, 4, 5] and is also a plausible hypothesis to explain the atmospheric neutrino problem [6].

The interpretation of the present experimental data in terms of neutrino oscillation is not a straightforward issue. Matter-enhanced oscillation [7] can naturally explain the solar neutrino deficit with parameters $\Delta m^2 = (0.3\text{–}1.2) \times 10^{-5}\ eV^2$ and $\sin^2(2\theta) = (0.4\text{–}1.2) \times 10^{-2}$ [8]. The atmospheric neutrino deficit requires parameters $\Delta m^2 >\sim 2 \times 10^{-3}\ eV^2$ and $\sin^2(2\theta) >\sim 0.56$. In addition, the recent claim from the LSND experiment [9] suggests the existence of $\nu_\mu \leftrightarrow \nu_e$ oscillation with $\Delta m^2 \sim 1\ eV^2$.

It is hard to accommodate the above parameters with three neutrino flavours [10, 11]. One can resort to radical explanations such as adding a fourth (sterile) neutrino [12] or disregarding some of the experimental evidence. Several scenarios have been proposed, differing in their initial assumptions and predicting rather different mass patterns [11, 13, 14, 15, 16, 17]. In addition, recent Cold-Hot Dark Matter (CHDM) models [18] prefer neutrino masses in the range of a few eV. The scenario with two light neutrinos and one heavy ν_τ in the mass range of $1 - 10\ eV$ is plausible. The CHORUS [20] and NOMAD [21] experiments, presently taking data at the SPS were inspired [19, 15] by the argument that a massive ν_τ is considered a good candidate for hot dark matter in the universe. Relating this mass of the ν_τ to the mass of the ν_μ by the see-saw mechanism the solar neutrino deficit would then also be explained.

In the near future, important new results are expected to shed some light on the experimental status of the various hints for neutrino oscillation. The SNO experiment [22], and in particular their measurement of the neutral current rate, can help to decide whether neutrino oscillation is the origin of the solar neutrino deficit. The Borexino experiment [23] can address the energy-dependence of the deficit, thereby constraining oscillation-based explanations. Forthcoming results from the Superkamiokande experiment and, in particular, more accurate results on the zenith angle dependence of the ν_e/ν_μ ratio, can clarify the atmospheric neutrino situation. The CHOOZ experiment [24] will soon measure the disappearance of $\bar{\nu_e}$ thus testing one of the possible origins of the atmospheric neutrino anomaly. More data from LSND will improve the understanding of their measurements and an independent check of the effect will also come from the recently upgraded KARMEN experiment [25].

CHORUS and NOMAD have recently reported no evidence for oscillation at the level of the present best limit [26] using only a small fraction of their available data. They will reach a sensitivity of $\sin^2 2\theta_{\mu\tau} \sim 2 \times 10^{-4}$ for $\Delta m^2 \geq 100\ eV^2$, corresponding, within the above framework, to a ν_τ with a mass of about $10\ eV$. Their sensitivity to a lighter ν_τ, in the range of $1-5\ eV$ is $\sin^2 2\theta_{\mu\tau} \sim 5 \times 10^{-2}$. This sensitivity can be greatly improved by a next-generation short base line experiment (SBLE). If oscillation occurs at the present best limit, CHORUS and NOMAD would each find 60 events. Even if a few τ^- candidates would be unambiguously detected, this would have strong implications to our understanding of the neutrino oscillation scenario. This would definitely call for a new high sensitivity exploration.

At present, a next generation of accelerator-based experiments is being planned to search for neutrino oscillation. At Fermilab, two new experiments, MINOS [27] and COSMOS [28] are approved.

MINOS is a long base line experiment (LBLE), which will use a beam from Fermilab to the Soudan Mine 730 km away, to test the hypothesis of neutrino oscillation with $\Delta m^2 \sim 10^{-2} - 10^{-3}\ eV^2$. COSMOS is a short base line experiment, similar in design to CHORUS, but expecting a total data sample one order of magnitude larger.

Several LBLE's [29, 30, 31] have been proposed using a beam from CERN to the Gran Sasso Laboratory in Italy, 732 km away. A combination of a LBLE and an intermediate base line experiment has also been proposed recently [32], which would use the present SPS beam and a detector of 400 tons located in the Jura mountain, 17 km from CERN, to explore neutrino oscillation in the region of $\Delta m^2 \sim 1\ eV^2$.

We believe that a next-generation $\nu_\mu(\nu_e) \leftrightarrow \nu_\tau$ short base line experiment (SBLE), in the CERN-SPS neutrino beam can be designed based on a hybrid detector. One can combine an emulsion target weighing a few tons and a high-resolution electronic tracker resulting in an experiment with 20 times more sensitivity than CHORUS and NOMAD and twice the sensitivity of COSMOS. Such an experiment will have a high discovery potential as it will be sensitive to $\Delta m^2 \sim 0.1\ eV^2$ at full mixing, while *simultaneously* being able to explore a domain of higher Δm^2 down to mixing angles of the order of $sin^2(2\theta) \sim 10^{-5}$. One hundred unambiguous τ^- events would be observed in this experiment if five events were detected in CHORUS and NOMAD.

Some analyses of present data suggest that $\nu_\mu(\nu_e) \leftrightarrow \nu_\tau$ oscillation may be found at a $\Delta m^2 \sim 1\ eV^2$ and with small effective mixing angle (*i.e.* $\sin^2 2\theta_{\mu\tau} \sim 0.06$). To illustrate this point we briefly describe in an appendix several recent studies which attempt to explain all presently available results. In this scenario this new SBLE will detect about 20 τ^- candidates.

In conclusion, neutrino oscillation is an appealing field of study, with a number of experiments either taking data or planned. The situation is rapidly evolving. New indications as to which regions are more relevant to be explored are expected to be refined in the near future. Candidate events from CHORUS and NOMAD will contribute to clarify the neutrino oscillation scenario, naturally calling for a follow-up experiment.

This document is organized as follows. In section 2 we briefly describe the activities at CERN which have lead to the design of this experiment. In section 3 we describe the improved SPS neutrino beam to be used by this experiment. In section 4 we present the basic design of the experiment and the principles of the search. The different detectors of the apparatus are described in section 5. Improvements still needing feasibility studies are presented in section 6. In section 7 we show the expected event selection efficiency, background estimates and the achievable results. These results are shown in terms of the expected exclusion plots to illustrate the reach of the experiment in a model-independent way. The conclusions are given in section 8.

2 A new short baseline experiment at CERN

At CERN, the neutrino community has recently reflected on a broad variety of options for future oscillation experiments. Several promising ideas, both for $\nu_\mu \leftrightarrow \nu_\tau$ and $\nu_\mu \leftrightarrow \nu_e$ oscillation searches, have been presented and discussed in a series of meetings and workshops held at CERN. Some of these have been published [33, 34, 35].

In this document we demonstrate that we can design an experiment which has high sensitivity for $\nu_\mu \leftrightarrow \nu_\tau$ oscillation and which will be capable of contributing significantly in clarifying the experimental scenario. This experiment will be ready to extend the investigation started with CHORUS and NOMAD, improving the sensitivity both in the mixing angle and in Δm^2. A combination of different approaches presented in the workshops has been retained as a baseline design.

It was pointed out [36] that a segmented emulsion target with passive material could allow a considerable increase of the target mass of the experiment. A solution (TENOR) was presented [34] to fit a segmented fully-sensitive large-mass ($\sim$ 5 tons) emulsion target in a magnetic field, complemented by high-precision silicon and emulsion trackers and by other more conventional electronic detectors. The use of silicon detectors on a large scale, as proposed in [33], allows high accuracy in the extrapolation of particle tracks to the emulsion target.

With a target mass in the order of a few tons, and exploiting the excellent and still improving performance of the SPS neutrino beam (see section 3), it is possible to collect about 5×10^6 charged-current neutrino interactions in three years. This large number of events can be scanned in its entirety without the need of kinematical preselection [34] owing to the recent advances in the technique of automatic emulsion scanning. This technique, pioneered by the group of Nagoya [37], has recently undergone further improvements. The Nagoya and Salerno groups of the CHORUS Collaboration have developed second generation automatic scanning systems [38, 39] able to cope with the request of the proposed experiment. The high spatial resolution of the silicon detectors can be used to restrict the surface area to be scanned, thus resulting in a significant reduction in scanning time [40].

A large rejection of background can be achieved by kinematical analysis of the candidate events using the knowledge of the direction of the τ^- before its decay. The need for a high efficiency on the measurement of momenta of charged tracks makes it mandatory to place the target in a magnetic field. We observe that in the past other experiments, such as WA17 [41] at CERN, have made use of emulsion stacks inside an intense magnetic field combined with external tracking.

In this Letter of Intent we will outline the design of such an experiment.

3 The CERN SPS neutrino beam

3.1 Introduction

The CERN West Area Neutrino Facility (WANF) [42] provides an essentially pure ν_μ beam. It has been in operation for over 20 years and was largely rebuilt in 1992-1993 [43, 44, 45] for the CHORUS and NOMAD experiments. It has now been operating for three years with record intensities. We propose a limited number of modifications to its present configuration which can be implemented using existing infrastructure and expertise, and with minimal additional expenditure.

3.2 The present neutrino beam

Fig. 1 shows a schematic layout of the present WANF beam line. Up to 1.5×10^{13} protons are extracted per spill using a fast/slow extraction from the SPS at 450 GeV in each of two 4 ms long spills separated by 2.6 s. Neutrinos are mainly produced by decays in flight of the secondary pions and kaons originating from proton interactions in a beryllium target (T9). Positive (negative) $\pi's$ and $K's$ are focused (defocused) towards the neutrino detectors by a horn and a reflector in front of a 290 m long vacuum decay tunnel. Protons which have not interacted, hadrons and muons

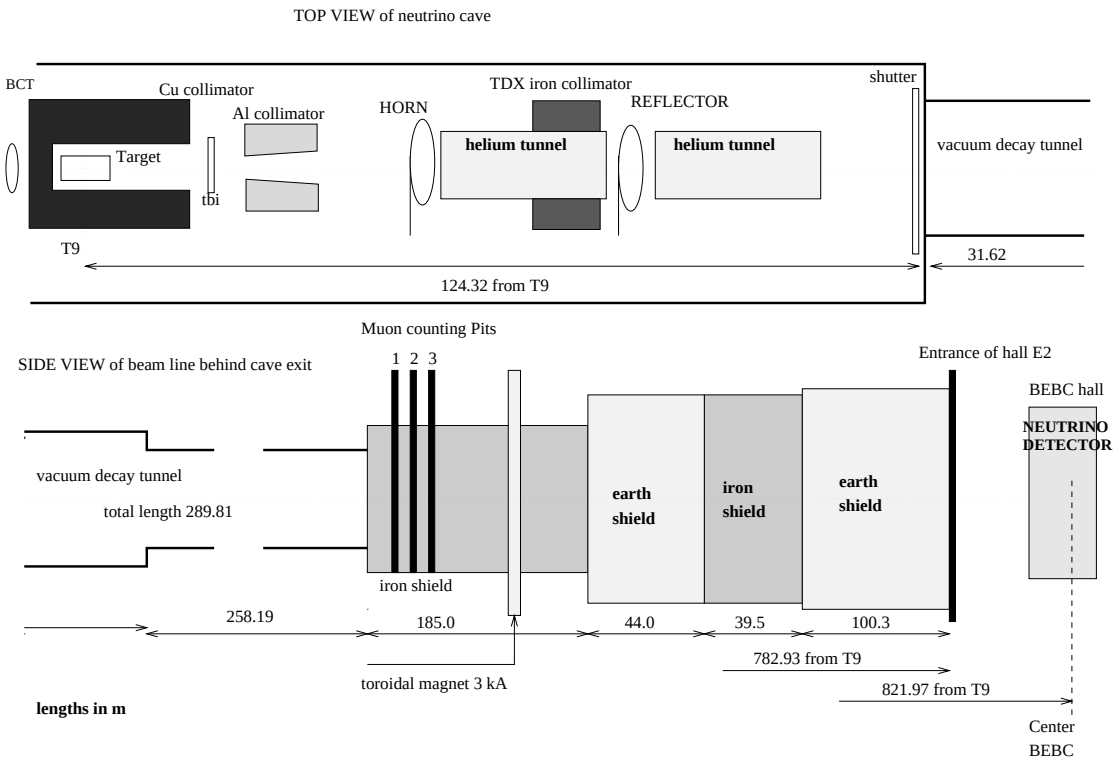

Figure 1: *Schematic layout of the WANF beam line pointing out its main elements (not drawn to scale).*

are absorbed by a 400 m shield of iron and earth. The neutrino detectors are housed in the BEBC Hall, about 820 m from T9.

The $\nu_\mu, \overline{\nu}_\mu, \nu_e$ and $\overline{\nu}_e$ flux at the detectors are predicted by detailed Monte Carlo simulations. The largest uncertainties in such simulations, *i.e.* particle production spectra in hadronic interactions, are expected to be reduced by the CHORUS and NOMAD data and by the results of the SPY experiment [46].

3.3 Prompt ν_τ background

The ν_τ contamination in the beam is the ultimate irreducible background for a $\nu_\mu \leftrightarrow \nu_\tau$ oscillation search. The largest contribution to this background comes from the prompt tauonic decay of the D_s produced from proton interactions in the neutrino target and inside the shielding.

Two new estimates of the ν_τ background have recently been published [47, 48], providing adequate knowledge of this background. They include the contribution from D_s^- (which is actually dominant), linear A-dependence of D_s production cross-sections, and a value for the D_s branching ratio as obtained in recent measurements.

For a proton energy E_{proton} of 450 GeV and the CHORUS detector fiducial volume, the two independent estimates of the ratio R of the number of ν_τ charged-current (CC) events to ν_μ CC events are 3.3 $\times$ 10^{-6} from the semi-empirical parametrisation of D_s production [47] and 3.5 $\times$ 10^{-6}

from the non-perturbative QCD approach [48], using the Quark-Gluon String Model (QGSM). The systematic uncertainties common to both approaches arising from the leptonic branching ratios, the D_s production cross-section and the model parameters amount to $\pm$ 30%.

This level of the prompt ν_τ background, still well below one event for the total duration of the CHORUS and NOMAD experiments, becomes more relevant for a future neutrino oscillation experiment aiming at improving the sensitivity by at least one order of magnitude.

An effective way to reduce the ν_τ prompt background is to lower the primary proton energy, thus exploiting the steep reduction of the D_s production cross-section and of the acceptance of the detector for prompt ν_τ. The number of ν_τ CC events per proton drops faster than the number of ν_μ CC events. A proton energy in the 300-350 GeV range is found to offer the best compromise. Assuming that the present WANF would operate at 350 GeV, the corresponding value of R is 1.2×10^{-6} [47], about 2.5 times lower than at E_{proton} of 450 GeV.

Additional experimental handles on the prompt ν_τ background are provided by the fact that D_s decays would result in an equal number of prompt ν_τ and $\overline{\nu}_\tau$ and that their energy spectrum is significantly harder than the one of ν_τ from the $\nu_\mu \leftrightarrow \nu_\tau$ oscillation.

3.4 Operation of a 350 GeV proton beam for neutrino physics

SPS protons originate in the PS proton linac (LINAC II) and are accelerated first in the PS Booster (PSB) and then in the PS itself. The PS and the SPS operate on a cycle which is a multiple of 1.2 s, given by the repetition time of the PSB. The PSB also sets the maximum intensity of about 3.0×10^{13} protons that can be accelerated in each PS cycle. Presently the SPS supercycle length is 14.4 s, corresponding to 12 PSB cycles of which two (16.7 %) are injected from the PS into the SPS at the beginning of the SPS supercycle. Due to beam emittance constraints, the SPS can accept only $\sim 2.3 \times 10^{13}$ protons per injection of which about 2.0×10^{13} are accelerated to 450 GeV, for a total of $\sim 4.0 \times 10^{13}$ protons per 14.4 s supercycle.

A number of modifications to the PSB and to the PS are foreseen to be implemented before the start-up of the LHC. Among the upgrades planned is the injection of the protons from the PSB to the PS at an energy of 1.4 GeV instead of the present 1.0 GeV. This would result in a reduction of beam losses owing to the lower emittance. The corresponding intensity of each injection from the PS into the SPS could therefore come closer to the PSB limit of 3.0×10^{13} protons. It is thus conceivable that in these improved conditions up to 4.5×10^{13} protons could be accelerated by the SPS per supercycle already before the year 2000.

A modified scheme of operation of the SPS has been worked out together with the CERN SL Division aiming at a realistic optimisation of the operation of the WANF and taking into account all the presently known operational constraints. Its guiding principles were

- In order to reduce the prompt ν_τ background, the energy of the protons impinging onto the neutrino target should be lowered to about 350 GeV.
- The proposed neutrino experiment should use the maximum possible proton intensity, by increasing the SPS repetition rate.

The following considerations were taken into account :

- Since the envisaged neutrino experiment is foreseen to be operational only after the decommissioning of LEP II, the lepton cycles (of total duration 4.8 s) will no longer be required. For the same reason a larger fraction of the PSB cycles could become available for injection into the SPS. The SPS repetition rate can be increased.
- A SPS cycle acceleration to 450 GeV will continue to be necessary for SPS experiments and test beams.
- These SPS experiments require a long flat-top (*i.e.* a slow extraction) presently 2.4 s
- The average power dissipation over the entire SPS supercycle must stay below the 33 MW limit. Since the SPS power dissipation is very high for the duration of the flat-top at 450 GeV enough time must be included at a lower power dissipation.
- A significant fraction of the total SPS proton intensity would be directed to the test beams and experiments on the 450 GeV flat-top. This will be more so the case after the start-up of COMPASS. The total number of protons on the targets T1, T2, T4, and T6 is foreseen to rise from the present 1.4×10^{13} to about 2.0×10^{13} per SPS supercycle once COMPASS [49] is also running.
- Sufficient time should be foreseen in the supercycle to allow for PS and SPS machine development cycles.

The proposed scheme, which satisfies all the above requirements is illustrated in Fig. 2.

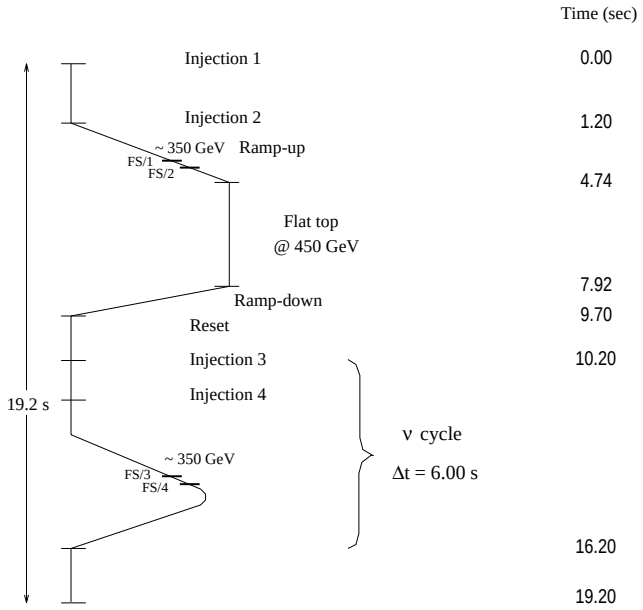

Figure 2: *Proposed SPS Supercycle.*

The proposed SPS supercycle duration is 19.2 s long, *i.e.* 16 PSB cycles, and consists of two sub-cycles. The first one, lasting 13.2 s with a 3.2 s flat-top at 450 GeV, is similar to the present one and will serve all targets. A second 6.0 s long sub-cycle will be introduced with just a bare acceleration cycle at 350 GeV, with no flat top, serving only the neutrino target T9, and power

Table 1: *Relative abundance of neutrino species*

	Average E_ν (GeV)	Relative Abundance	ν CC Events
ν_μ	25.0	1.000	1.94×10^6
$\overline{\nu}_\mu$	20.7	0.052	0.433×10^5
ν_e	37.4	0.0079	0.230×10^5
$\overline{\nu}_e$	29.4	0.0018	0.212×10^4

consumption level low enough to compensate for the longer flat top at 450 GeV. The duty cycle for the 450 GeV flat-top (3.2 s every 19.2 s) is very similar to the present one.

Two fast-slow extractions for neutrino physics (FS/1 and FS/2) would take place at about 350 GeV on the ramp-up of the first sub-cycle. These two spills are separated by about 100 ms, *i.e.* about 10 GeV energy difference. Another two fast-slow extractions (FS/3 and FS/4) would take place in the dedicated neutrino sub-cycle at energies identical to FS/1 and FS/2. Such a SPS supercycle also accommodates the necessary spare time to allow for PS and SPS machine development cycles.

The neutrino target could be served with about 2.5×10^{13} out of 4.5×10^{13} accelerated protons in the first subcycle. It will certainly be able to withstand at least 3.9×10^{13} protons in the second subcycle. The total is then 6.4×10^{13} protons per supercycle. The overall gain with respect to the present WANF configuration amounts to about a factor of two in terms of protons per unit time. However, we plan to investigate if the present target, or possibly a new target made of carbon, could withstand in the second sub-cycle more or all of the available intensity of 4.5×10^{13} protons.

Currently, the focusing elements (horn and reflector) fire twice within a SPS supercycle with a separation of ~ 2.6 s. In the scheme presented above, the horn and the reflector need to refire with a short 100 ms time separation. The first tests of such conditions have proven very successful. Four fast-slow extractions for neutrino physics within the 19.2 s SPS supercycle will therefore be possible.

3.5 Expected performance of the upgraded WANF

Fig. 3 shows the predicted energy spectra for each neutrino flavour for the upgraded WANF. Tab. 1 gives the average energies, contamination and expected number of events for the envisaged experiment and for a one year run consisting of 200 days. We assume that the total number of protons on target is 4.3×10^{19} per year, and that the fiducial target mass and area are 2.4 tons and 1.44×1.44 m^2, respectively. A global efficiency of 75% has been taken into account.

Further improvements for the WANF are expected by:

- optimising the horn and reflector for a proton energy of 350 GeV thus increasing the neutrino flux, and
- developing a carbon-based target able to withstand the full intensity 7.0×10^{13} per 19.2 s SPS supercycle.

A new neutrino facility (NuMI) is being planned using a proton beam from the Fermilab Main Injector. A short base line experiment (COSMOS) on the Fermilab site would search for $\nu_\mu \leftrightarrow \nu_\tau$ oscillation. Thanks to its higher repetition rate (1.9 s compared to 19.2 s cycle length at the SPS)

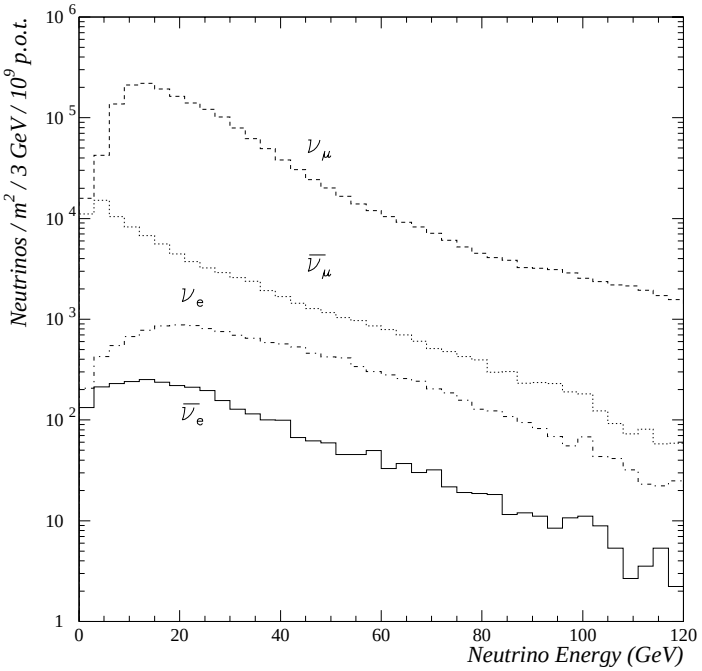

Figure 3: *The predicted neutrino energy spectra at the position of the detector for a 350 GeV proton beam.*

and the longer running time per year (300 days) envisaged, the NuMI is expected to provide about 8 times more protons per year than the WANF. However, the higher proton energy of the SPS (350 GeV compared to 120 GeV) compensates this difference to a large extent. The higher proton energy results in a higher ν_μ production efficiency and interaction probability. For a $\nu_\mu \leftrightarrow \nu_\tau$ search an additional factor of ~ 3 comes from the strong suppression of ν_τ interaction probability at the lower energy. The envisaged short baseline station at NuMI is only 1.5 times better than the one at CERN. If also the larger detector fiducial mass (2.4 tons compared to 0.8 tons for COSMOS) is taken into account the experiment described here would obtain per year 1.0×10^6 effective CC interactions above ν_τ threshold to be compared to 0.5×10^6 per year projected for the COSMOS experiment.

3.6 Time constraints for the experiment

A future neutrino experiment would have to fit into the overall CERN machine schedule. In particular, the following constraints must be taken into account:

- It is foreseen that disruptions to the SPS operation will be introduced in 1999 as a consequence of the LHC civil engineering related to the excavation of the shafts and caverns for the experiments. The estimated SPS down-time in 1999 due to the re-alignment of the SPS caused by the excavations is about 60 hours (7 interventions each of about 8 hours duration) [50].

- In addition, the SPS supercycle presented above assumes that a future neutrino experiment would be operational only after the end of LEP II. The last year of approved LEP II operation

is 1999.

Therefore, the year 2000 seems to be the earliest full year at which a next generation neutrino experiment could take data. It should be remembered that a fraction of this year would be devoted to the excavation of the transfer line from the SPS to the LHC but a neutrino experiment could be scheduled around this work.

4 Design of the experiment

4.1 Outline

It is the aim of this experiment to reach a sensitivity for $\nu_\mu \leftrightarrow \nu_\tau$ oscillation which is at least an order of magnitude better than that achieved in present experiments. Therefore, an increase of the event rate by a similar factor must be achieved while retaining a negligible background. As a consequence, the background rejection must also improve by an order of magnitude.

A baseline design will be described for a detector capable of reaching the above goals. This design adopts a conservative approach implementing well known and proven techniques. The design is based on the experience accumulated in the CHORUS and NOMAD experiments. It exploits the basic ideas described in the introduction, as derived from studies as in [33] and [34] and discussed in the recent Workshops at CERN.

This design calls for a hybrid detector with a massive target composed of nuclear emulsion followed by high precision silicon microstrip detectors, both placed in a magnetic field and surrounded by an efficient muon detection system. These choices will be justified below.

Optional optimizations will also be explored. It is expected that these will make it possible to enhance the sensitivity of the experiment by increasing the efficiency or the ability to implement more target mass. Some of the features adopted in these approaches need to be supported by results of test experiments, planned to be performed at the CERN PS in September 1997.

4.2 Principle of the measurement

The existence of neutrino oscillation is inferred from the occurrence of charged-current (CC) interactions of τ-neutrinos in the detector:

$$\nu_\tau N \;\rightarrow\; \tau^- X.$$

The detection of the tau lepton in the final state identifies this reaction. The τ^- is detected through its decay modes into muons, hadrons and electrons:

$$\tau^- \rightarrow \mu^- \nu_\tau \overline{\nu}_\mu,$$

$$\tau^- \rightarrow h^- \nu_\tau (n\pi^0),$$

$$\tau^- \rightarrow \pi^+ \pi^- \pi^- \nu_\tau (n\pi^0),$$

$$\tau^- \rightarrow e^- \nu_\tau \overline{\nu}_e.$$

The τ^- identification is carried out by making use of its characteristic decay topology, by the charge measurement of its decay products, by its distinct decay kinematics and by the missing energy carried away by the neutrino(s) in the decay process. In about 85% of the cases the τ decays into a single charged particle and in most of the remaining cases into three charged particles.

4.3 Background processes

We first present an overview of background processes which could simulate the presence of a CC ν_τ interaction. We then explore the strategy to distinguish background from the signal. This approach leads us to a set of requirements for a detector. A more detailed quantitative study of the number of background events will be described in a following section.

The most abundant events in the detector are inclusive CC interactions of ν_μ. They have a negatively charged muon in the final state, which does not produce a decay topology, nor a sizable missing energy. Only processes with a special topology, such as charm production can be confused with events with a τ in the final state. Decays of the primary muon or of pions and kaons are easily rejected by the requirement of a minimum decay transverse momentum.

Charmed particles produced in ν_μ and ν_e CC interactions decay with a lifetime similar to the τ^-, but can be distinguished from τ^- by their positive charge. Negatively charged charmed particles can be produced in the charged-current interactions of $\overline{\nu}_\mu$ and $\overline{\nu}_e$. The additional presence of a μ^+ or e^+ allows to reject these events. In the cases where the primary leptons are not identified, kinematical criteria can be used as further reduction. In particular, the presence of a K^0 in their decay products can be used to discriminate these events from τ-decays.

Another source of negatively charged charmed particles is the associated charm production in neutral-current (NC) reactions. These events are rare and can be suppressed by the detection of a second decay topology in the same event. A powerful rejection can be obtained by comparing the direction of the missing energy as predicted from the decay angle with the total transverse momentum vector of the event. The latter is dominated by the unmeasured primary neutrino momentum, and is uncorrelated with the decay topology.

Neutral-current interactions without charmed particle production can only simulate a decay topology, when one of the negatively charged hadrons interacts close to the primary interaction vertex. Only a very small part of these secondary interactions have no additional visible activity. These are called "white kinks" in emulsion terminology. These events do not exhibit the characteristic decay kinematics. CC interactions with white kinks are rejected making use of the presence of the primary lepton. Although the kinematics of the remaining events is more similar to that of ν_τ CC events than the NC events with white kinks, it is expected that their final contribution to the background is negligible.

4.4 Requirements for the detector

The arguments given above show that a sensitive experiment must have the following properties.

- The product of target mass, neutrino flux and τ-detection efficiency has to be at least ten times larger than in the present experiments. As shown above, the optimized operation of the neutrino beam can provide a doubling of the integrated flux without loss to the other users of the SPS. An increase of a factor of (at least) three in target mass and an increase of a factor three in τ-detection efficiency with respect to CHORUS is then required.
- The irreducible background of prompt ν_τ in the beam can be brought to an acceptable level by lowering the proton beam energy and by rejecting high energy events. This has been shown to be feasible (section 3).
- Tracking detectors must ensure an efficient event reconstruction.

- The massive target has to allow for a unique detection of the decay topology. One notes that the characteristic τ^- decay length at the SPS energy is 1 mm.
- The charge of the candidate decay daughter(s) must be determined unambiguously.
- Muons and electrons have to be efficiently identified.
- The kinematics of the event must be determined. In particular, a measurement of the magnitude and direction of the decay daughter momentum, of the missing energy, of the hadronic shower, and the parent particle direction must be obtained. This requirement leads to a design where the momenta of all charged particles are well measured, and calorimetry may be employed to have full coverage of the energy flow of neutral particles.

4.5 Detector choices

A nuclear emulsion stack, made up of plates, can provide an efficient and background-free detection of the decay topology as well as a large target mass. With this technique, the decay can be visualized and the details of the decay topology ("kink" in the track) can be studied. A unique feature is the three-dimensional nature of the information provided. Also the availability of extremely fine detail gives full efficiency for the detection of all charged tracks emerging from the reaction, and the possibility of electron identification. This provides a strong rejection of kinks produced in nuclear interactions by hadrons. Nuclear emulsion is the only known technique which can also provide a measurement of the direction and track length of the parent particle. The design follows the methods developed in CHORUS [20].

The emulsion will be scanned by fully automatic microscopes. The method is to use high precision predictions onto the downstream face of the emulsion, and to scan back plate by plate. This method is being used in the CHORUS experiment. Recent advances in the fast microscope technology have made it possible to increase the scanning speed to the level that all events can be searched for kinks. No kinematical preselection of events is necessary, thereby avoiding losses in the selection process, thus keeping high efficiency for τ^- events.

A tracker composed of silicon microstrip detectors allows for a high-precision prediction of the event location in the emulsion. In combination with other tracking detectors, they are a powerful ingredient in the event reconstruction and charge and momentum measurement of charged particles. Silicon microstrip detectors combine good time resolution with excellent position and two-track resolution. The high resolution track extrapolation from the silicon detectors to the emulsion target allows to scan a smaller emulsion surface, contributing to effectively reduce the scanning time per event as compared to CHORUS. This experiment uses a configuration similar to the one presently being constructed for the NOMAD-STAR project [40].

The magnetic field, necessary for the determination of the charge of the decay daughter and for momentum analysis of all charged particles, is provided by the UA1 magnet, presently in use in the NOMAD experiment [21].

The large surface tracking detection inside the magnetic field is provided by honeycomb chambers, with a design similar to the tracking planes recently installed in the CHORUS apparatus [51]. These detectors are needed for pattern recognition, charge and momentum determination and muon identification.

Part of the present instrumentation of the NOMAD experiment, such as the electromagnetic calorimeter, external muon identification and hadron calorimeter will be reused. Additional chambers inside the magnet yoke extend the identification of muons to the large-angle region.

5 Description of the detector

5.1 Modular design

The inner part of the detector is composed of six equal modules, each containing an emulsion target 6 cm (2 radiation length) thick, a set of silicon trackers and a set of honeycomb tracker planes (Fig. 4). Each module provides an active mass of emulsion of 400 kg. The total length of a module is 1 m, thus providing sufficient space to perform pattern recognition with the tracking detectors and to determine the momentum and charge of particles. The six modules are followed by the electromagnetic calorimeter. Modules and calorimeter together are mounted inside the magnet.

The magnet is followed by a hadronic calorimeter and by two muon identification stations separated by an 80 cm iron absorber and composed of drift chambers.

The trigger uses a combination of signals from the silicon and wire chambers. The trigger requirement is based on combinations within one target module in order to ensure good homogeneity of the trigger efficiency.

5.2 The emulsion target and scanning procedure

The design of the emulsion target follows closely the experience gained with the CHORUS experiment. The thickness of each target stack is 60 mm, equal to the amount of material between each tracking section in CHORUS. Each of the modules contains four emulsion target blocks, mounted in a two by two matrix. In a plane perpendicular to the beam these blocks form a square with sides of 72 cm and match the size of the silicon tracker to which they can be fixed mechanically with high precision. This ensures excellent alignment of the two systems. The blocks are built from two stacks of target emulsion plates, which have the same dimension as the CHORUS emulsion (72×36 cm^2). The dimensions match the existing emulsion pouring and development facilities and the automatic microscope stages.

The emulsion stacks are made of 72 target emulsion plates (Fig. 5). Each target plate is composed of a thin backing layer, of about 100 μm thickness with 350 μm emulsion layers on both sides. Ionizing particles induce a latent image of their track in the emulsion material. After development, this provides 300 black grains per mm of track trajectory, which contain position information with a 0.3 μm precision. In routine scanning the position accuracy to locate the grains is 1 μm.

Special emulsion plates are added to the downstream end of the target stacks, to provide higher angular resolution for the connection of the tracks found in the electronic detectors with the target stack. These special plates consist of two 100 μm emulsion layers separated by an 800 μm thick backing layer. Scanning systems can measure the angle of tracks from the grains found on both sides of the backing layer with a precision of about 1 $mrad$.

The entire emulsion target, together with the associated electronic trackers, is placed in a "cool box" with controlled temperature ($\sim 5^0$C) and humidity. This is to prevent the loss of the latent image in the emulsion (fading) during the running time of the experiment.

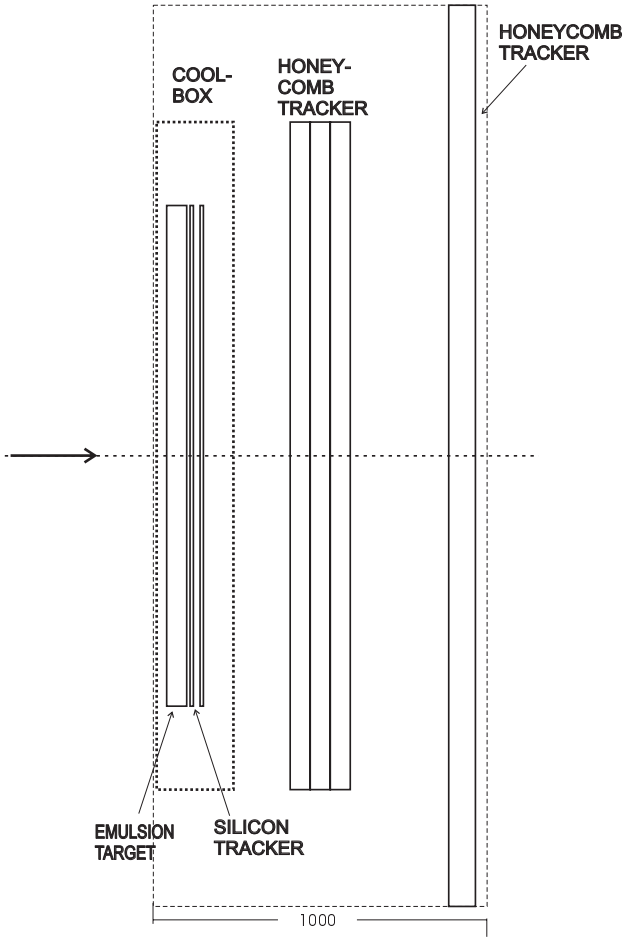

Figure 4: *Schematic view of one target module with the emulsion and the tracking detectors.*

Possible background sources are well under control. The effect of cosmic-ray tracks is strongly reduced by keeping the undeveloped emulsion plates vertical. The background induced by muons associated with the neutrino beam and with the SPS X7 test beam are kept at an acceptable level. In particular, those muons are used for emulsion alignment purposes. The possible background produced by showering tracks in neutrino events is negligible in CHORUS and it is expected to remain at a very low level in this experiment (less than one shower track per microscope view).

Events are located in the emulsion target by a scan-back method [37, 38, 39]. The electronic tracking detectors provide a precise prediction of the exit point and direction of all suitable tracks of the event. A track is suitable for scan-back when its momentum is above 1 GeV/c and its angle is smaller than 400 $mrad$ with respect to the beam axis. These tracks are then searched for in the special plates. The position resolution is determined by the precision of the silicon microstrip detectors and by the alignment accuracy. We estimate that the alignment limits the matching precision to 20 μm (at one standard deviation). The angular prediction accuracy can be matched to the 1 $mrad$ resolution of the special plate and is dominated by multiple scattering in the silicon detectors. A schematic drawing of the track location method in the special emulsion plates is shown in Fig. 6.

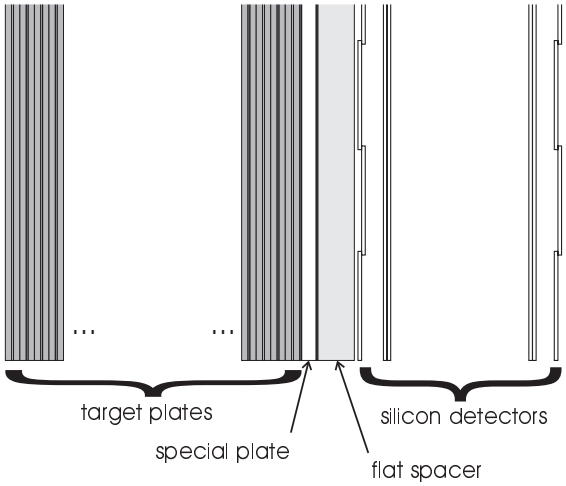

Figure 5: *Schematic drawing of a target emulsion stack and silicon trackers.*

The precision of the prediction is not much altered by the presence of a magnetic field, for particle momenta above 1 GeV/c as long as the distance between the tracking detector and the emulsion plate does not exceed 20 mm. When compared to the CHORUS situation, the volume of phase-space defined by the position and angular accuracy of the predicted track is two orders of magnitude smaller, allowing for a higher beam intensity and longer exposure time before background of randomly matching tracks becomes a problem. Over 90% of the events have suitable tracks for location. These are followed in the upstream plates, plate by plate, until the interaction vertex is found. High momentum tracks are used to perform correction of local track distortions caused by the emulsion handling. This procedure is not affected by the magnetic field since it is applied to track segments of ≈ 100 μm length.

As already discussed, we aim at an improvement of the scanning time with respect to CHORUS, due to a more accurate prediction of the track coordinates in the emulsions. A reduction of about a factor 100 in the special plate surface to be scanned is achievable because of the precise predictions of the silicon detectors.

We mentioned that systems have been developed to fully automatize the emulsion scanning procedure. At present, two types of automatic microscopes exist, which differ in implementation features [38][39]. The systems function as follows. An emulsion plate is mounted on a movable stage, with mechanical precision of 0.5 μm. The position is controlled by a PC through a motor controller. The plate is moved to the relevant position with respect to the microscope objective. The focal plane of this objective can image small slices of the emulsion layer, such that for a single track an independent measurement of its position can be obtained each 6 μm. By a vertical movement of the objective, multiple slices of the emulsion layer can be brought into focus. The optical image is digitized with the help of a CCD camera and the digital image is made available to a processor. The combination of many layers of images, obtained by focusing different depths into the emulsion layer is input to a track finding algorithm. On special plates, about 16 independent layers can be measured on each side of the backing. Tracks are found by requiring consistency on both sides of the backing. The target stacks are then used to scan-back tracks predicted with the special plates. The interaction vertex can be located with this method.

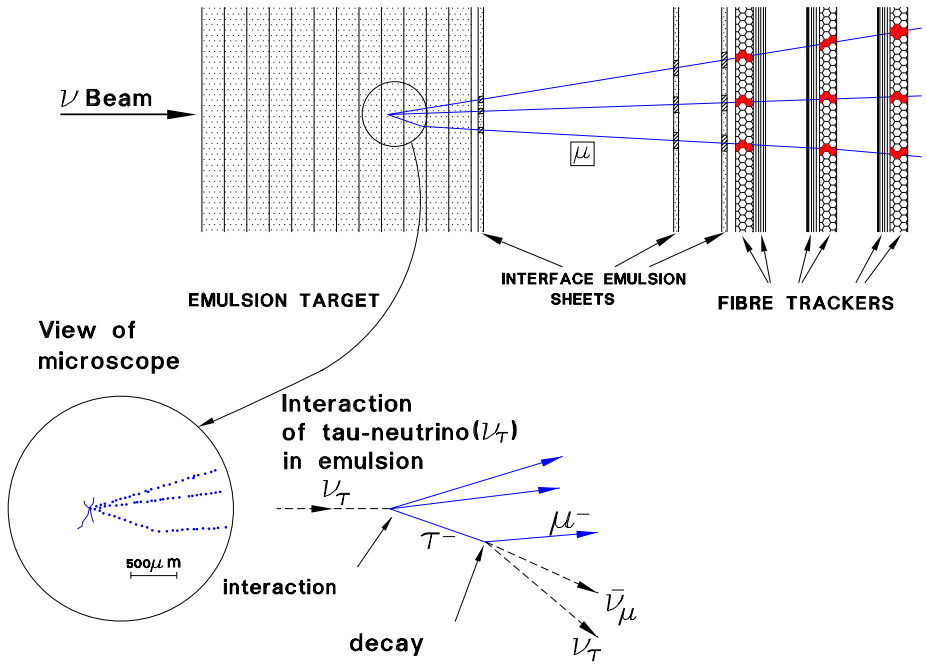

Figure 6: *Event location in the CHORUS experiment.*

The scanning capability now achieved by CHORUS is about 10^3 events / (month × microscope), including the operational efficiency. Most of the scanning time goes into the analysis of the special plates downstream of the target emulsion. Using the information from these plates, the tracks in the target can be located with a micron accuracy. The complete emulsion event reconstruction is performed only for those events with a decay topology (tau or charm decay).

The speed with which the automatic system can process one event depends ultimately on the speed with which pixels can be extracted from a CCD and the accuracy of the prediction. With reasonable extrapolation of recent advances in this technology, an estimate of the scanning time per followed track is one second per emulsion plate traversed. We assume that 20 automatic microscopes will be available and will be routinely operated with the tools and the experience now being gathered. With the improvements quoted above, a scanning capability of about 3×10^6 events/year is feasible. As already pointed out, the full measurement of the plates in a target module will be done only for candidate events. The scanning of 2×10^6 muonless and 6×10^6 muonic events appears feasible in about two years after the end of the data taking. In that sample, the fraction of events to be completely reconstructed can be estimated, from charm production, to be about 5%. A simplified model of an automatic scanning system is shown in Fig. 7.

Techniques now exist to fully digitize the volume around the interaction vertex, and to perform pattern recognition on this information. The emulsion can then be regarded as a succession of two-dimensional tracker planes, 6 μm apart with a point precision of about 1 μm. Decay kinks with kink-angles larger than 10 *mrad* can be measured in the emulsion target. This technique also allows to measure the direction of the decay parent, which is extemely valuable for the study of the decay kinematics. All other charged tracks emerging from the vertex are also visible, and their track parameters can be measured (Fig. 8). Corrections for distortions in the emulsion can be performed using through-going tracks near the vertex (see Fig. 8).

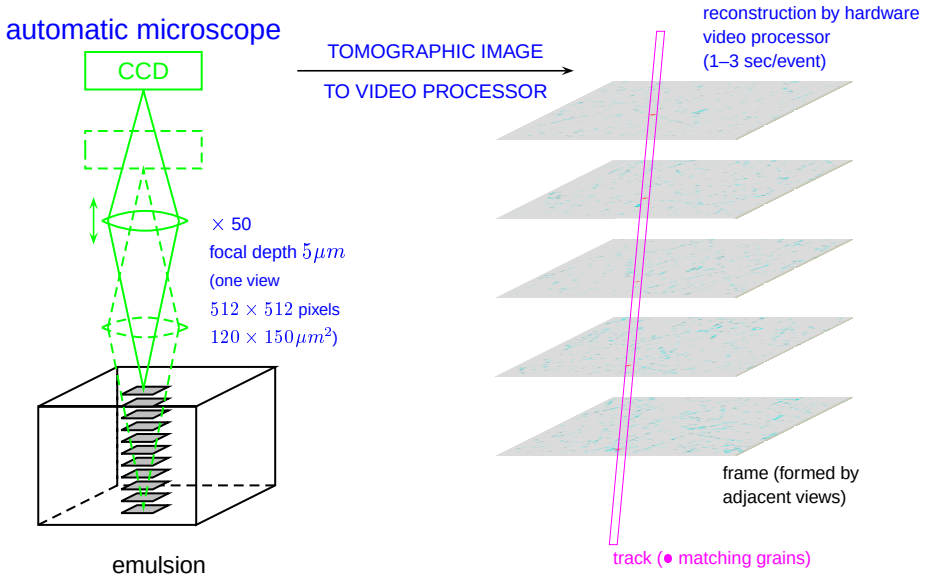

Figure 7: *Schematic drawing of an automatic microscope stage.*

5.3 The silicon microstrip detector

The main purpose of the silicon tracker is to provide a precise interface between the emulsion target and the other electronic trackers. Therefore, it must provide a space segment, which gives efficient pattern recognition in the electronic tracker providing a high resolution constraint. It also allows good momentum resolution and gives a precise prediction of the track impact point in the emulsion. In fact, the ultimate precision of silicon microstrip detectors is about 20 microns, limited by multiple scattering in the silicon itself and in their support and by aligment uncertainties. This allows the track prediction in the emulsion to be within one microscope view (about 100×100 μm^2) at the 5 σ level. In comparison with CHORUS, this represents a reduction of about a factor 100. This is important not only to achieve a much higher scanning speed, but also to reduce backgrounds associated with randomly matched tracks.

In order to provide a segment, two $X-Y$ points are needed. The silicon tracker consists of two planes (each plane is defined as providing an X-Y measurement). The first plane is located as close a possible to the emulsion (10 mm) while the second plane is at about 50 mm from the emulsion to provide a sufficiently long lever arm.

Each plane consists of two layers of single-sided silicon microstrip detectors. The first layer has strips pointing in the direction perpendicular to the magnetic bending plane, while the second layer strips are perpendicular to the first one. The two layers are mounted very close to each other, in order to minimize error in the second layer due to multiple scattering in the first. From this point of view, the use of double sided detectors or back-to-back glued detectors would seem preferable. However, there are several reasons to use independent layers of single sided detectors: the construction of the detector modules ("ladders") is much simpler, the detectors and modules are more robust and the signal to noise ratio of the two layers is the same. In the case of double sided detectors the extra capacitance of the n-side results in a degraded performance.

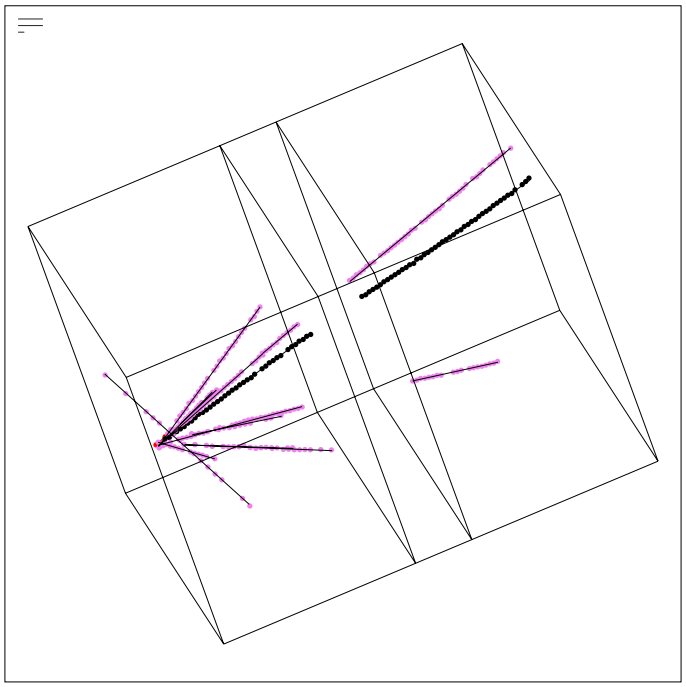

Figure 8: *Reconstructed event measured in the CHORUS emulsion. Shown are the grains, with reconstructed tracks, in the emulsion layers on both sides of the plastic backing. To indicate the scale, the sensitive volumes (emulsion layers) have a thickness of 350 μm each, and the plastic backing 100 μm. A background track not related to the event is also displayed.*

Each layer consists of 48 half modules. A half module is made up of 12 individual detectors, $6.1 \times 6.1\ cm^2$ in surface, 350 μm thick, glued together to a common carbon fiber back-bone and wire-bonded. One end of the module is glued to a hybrid board containing the read-out electronics. Two half modules are glued (at the end opposite to the electronics) to form a full "ladder" 1.44 m long. The read-out electronics is at both ends of the ladder outside the fiducial volume. Twenty-four such ladders, slightly overlapping with each other form a layer of active dimensions of $1.44 \times 1.44\ m^2$. The second layer is fixed to the same support frame as the first one, and has the same structure, except that the ladders point in a direction perpendicular to the ladders of the first plane. A plane is made up of 48 ladders, and therefore the silicon tracker of each one of the 6 independent modules in the detector consists of 96 ladders. The total number of ladders is 576.

The design and operation of the silicon tracker relies largely on the experience acquired with the NOMAD-STAR project [40]. In fact, very long (72 cm) ladders with good signal to noise ratio have already been succesfully and reliably built. This detector will be installed in March 1997 right upstream of the NOMAD first drift chamber. It consists of 4 layers of passive material, boron carbide (B_4C, $X_0 = 22\ cm$, $\rho = 2.5\ g/cm^3$) each followed by a layer of single-sided silicon microstrip detectors, plus an additional layer at the end. The 5 layers of silicon detectors (for a total active surface of about 1.14 m^2) allow the measurement of the track coordinates in the projection parallel to the magnetic field. Each layer consists of 10 overlapping ladders made of 12 independent detectors (Fig. 9). A total of 50 long ladders have been built. The design of the half modules proposed here

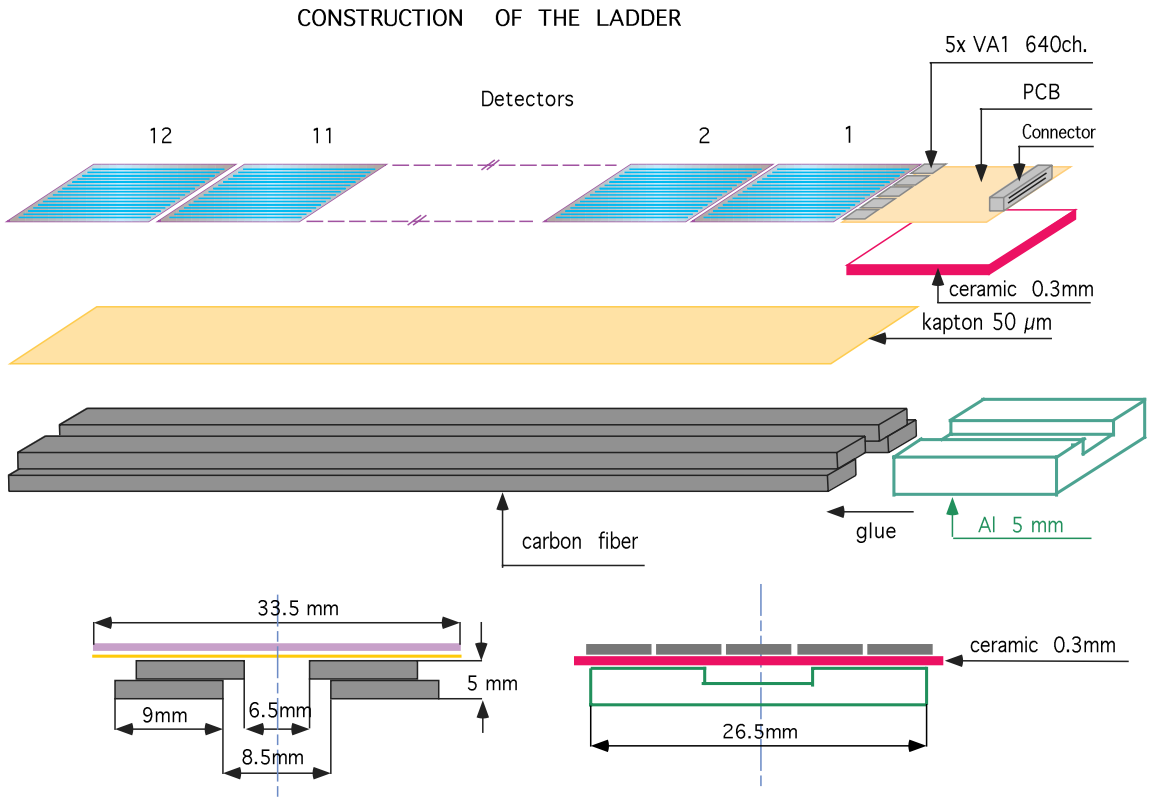

Figure 9: *Schematic drawing of the 12-detector STAR silicon ladders.*

is very close to the STAR ladders.

The construction of the STAR detector has already provided valuable experience, as well as infrastructure. A fully equipped silicon laboratory at CERN (shared with the OPAL and CMS silicon groups) has been used to build the STAR detectors in a very short period of only 6 months. The performance of the ladders is excellent. The signal to noise ratio of the ladders is 15-16, and a spatial resolution better than 5 μm has been measured. The number of defective channels is less than 1 %. The ladders are mechanically robust, and the read-out electronics (the VA1 chip, a commercial descendent of the VIKING has been used [40]) performs very well. During production, two ladders a day were built. Detector testing, mounting of the ladders and debugging was done in parallel. The STAR detectors manufactured by Hamamatsu are AC coupled, FOXFET biased [52], single sided wafers of 60×33 mm^2 transverse dimension and 325 μm thickness, with a read-out pitch of 50 μm and a floating strip at a pitch of 25 μm. The detectors were selected applying the following criteria: good quality (low leakage current and small number of defects), simplicity (single sided) and availability (the masks and the production chain were available from Hamamatsu, thus eliminating development costs and guaranteeing prompt delivery). The detectors were purchased at a very competitive price, 15 SF/cm^2.

Our baseline design for this detector simply doubles the dimensions of the detectors and the pitch keeping the basic features of the STAR ladders. A resolution better than 10 μm is achieved by using a pitch of 100 μm with a floating strip at 50 μm. Following the STAR experience, the construction

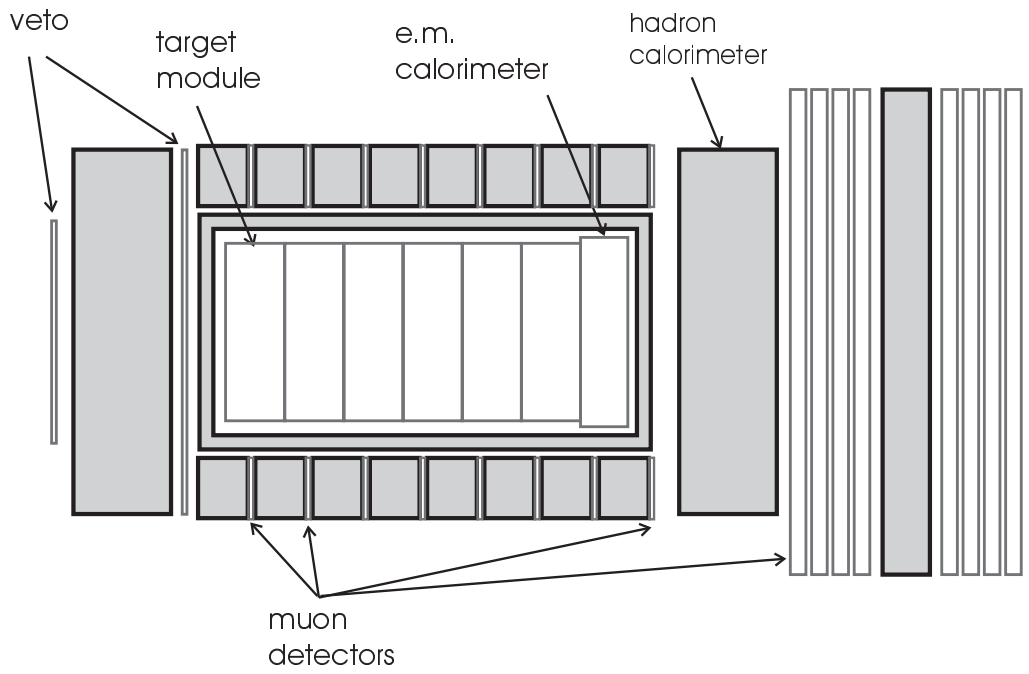

Figure 10: *The UA1 magnet with the detector elements inserted for this experiment.*

of two half-modules a day (one ladder) is possible. We need 576 days for the full detector, the production of which can be spread over a period from two to three years. The time scale can be improved if several groups participate in the construction of the silicon system.

We are confident that the silicon tracker needed for this experiment can be built in a reasonable time and at a moderate cost, in spite of its large dimensions. Considerable experience has been gathered with the construction of the STAR detector and will further improve with its commissioning and operation during the 1997 run.

5.4 The magnet

The magnet is the UA1 dipole currently being used in NOMAD (Fig. 10). It has an inner field volume of $7.5 \times 3.5 \times 3.5$ m^3. It provides a horizontal field of up to $0.7\ T$ in a direction perpendicular to the neutrino beam. The magnet consists of mirror-image halves (the plane of symmetry is a vertical plane containing the beam direction) which open on a system of rails to give access to the detector. Each half consists of 8 iron C's, providing the return path for the magnetic field, and one water cooled aluminium coil. Each C is 87.5 *cm* long along the beam and successive C's are separated from each other by 80 *mm* gaps.

5.5 The honeycomb chambers

Each target module contains a large-surface tracking section composed of honeycomb chambers. These chambers are similar to the ones installed in 1996 in CHORUS (Fig. 11)[51]. They are made up of closed hexagonal cells with a size of approximately 1 cm and with a pitch of 1.2 cm. Each cell has a thin (20 μm) sense wire at about 2000 V potential difference w.r.t. the wall of the cell. This wall is made of preformed conductive plastic. The operation of these chambers is similar to straw tubes. The difference is that the construction of large planes is easier, since wires can be positioned when the cells are still open.

Three orientations will be constructed rotated at 60 degrees with respect to each other. Each orientation contains six wire planes. This is sufficient to perform pattern recognition and to obtain three-dimensional information. In the magnetic bending-plane additional wire planes are employed to increase the momentum measurement capability. An electronic design is available for these chambers, where each wire is connected to its own multi-hit TDC. The precision which can be reached in large systems is 200 μm per plane.

For a momentum determination employing measurements in one single module, combining silicon and honeycomb trackers, we estimate a total momentum resolution below 10% up to 25 GeV/c.

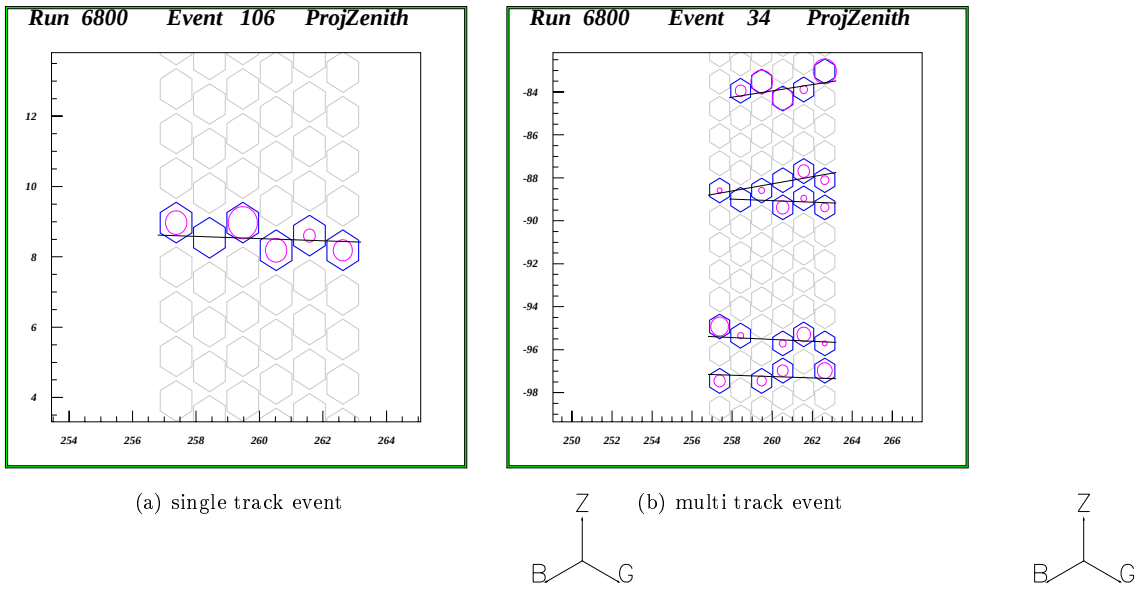

(a) single track event (b) multi track event

Figure 11: *Single and multi track events measured in the CHORUS honeycomb chambers.*

5.6 Muon detection

This system consists of the one presently used in NOMAD and located at the end of its apparatus, complemented by an additional muon detector to provide coverage at large angles. The latter is necessary to enhance the identification of positive muons accompanying negative charmed particles produced by $\overline{\nu}_\mu$. The present system consists of 3.75×5.55 m^2 drift chambers each made of two planes of vertical and two planes of horizontal drift tubes. The detectors are assembled in modules

of two chambers. The first muon detection station consists of three modules and is placed behind the hadron calorimeter. It is followed by an 80 cm thick iron absorber and a second muon station of two modules. The chambers are operated with a 40-60 Argon-Ethane mixture and have a position resolution of 450 μm.

The magnet return yoke, described above, consists of 8 C's on each side of the magnet each 87.5 cm long along the beam (Fig. 10). Planes of streamer tubes are inserted in the 80 mm gaps between successive C's. These provides muon identification after they traverse part of the iron of the C's. In order to be detected in two successive planes of streamer tubes, a muon must have a momentum of at least 1.4 GeV/c. In the subsequent discussion on the background it has been assumed that muons with momenta greater than 2 GeV/c are identified. Fitting the 7 gaps with single planes of streamer tubes would result in a 5152 channel system of standard technology. A similar system would be designed to instrument the downstream end of the magnet just behind the hadron calorimeter.

5.7 Preshower and electromagnetic calorimeter

The preshower and electromagnetic calorimeter, currently used in NOMAD, are needed to recognize and reconstruct electrons and photons produced in the last emulsion stacks. The calorimeter is made of 875 lead glass blocks each 19 radiation lengths deep and with a rectangular cross-section of 79×112 mm^2. It is preceded by a preshower consisting of two planes of proportional tubes following a 9 mm thick (1.6 X_0) lead-antimony converter. The preshower provides a better position measurement of photons converting in the lead and electron-pion discrimination based on the early shower development technique. The preshower consists of 286 horizontal and 288 vertical tubes made of extruded aluminium profiles. Each tube has a cross-section of 9×9 mm^2 and a wall thickness of 1 mm and is strung with a 30 μm gold-plated tungsten anode wire held at a tension of 1500 V. The tubes use an 80-20 Argon $-$ CO_2 mixture. The variation of the preshower gain with temperature and pressure is monitored using the pulse height of straight through muons.

The lead glass counters (of type TF1-000) have to operate in the magnetic field perpendicular to the counter axis. Each block is read by a tetrode with a typical gain of 40 optically coupled to the back face of the block. This face is cut at 45^o with respect to the counter axis, such that the axis of the tetrode forms an angle of 45^o to the field direction. This limits the signal reduction due to the effect of the magnetic field to 20 %. Monitoring of the lead glass response is performed using two blue LED's for each block. The energy resolution of the calorimeter was measured to be $\Delta E/E = (1.0 \oplus 3.2/\sqrt{E})\%$ where E is expressed in GeV. It was also found to be linear to better than 1.5 % in the energy range 1.5 to 80 GeV.

5.8 Hadron calorimeter

The hadron calorimeter, currently used in NOMAD, measures the energy and direction of neutral hadrons and provides a confirmation of the energy of charged hadrons as measured by the trackers. It is made of eleven 4.9 cm iron plates interleaved with 1 cm thick scintillator and has an overall area of 3.6×3.5 m^2 and a thickness of 3.1 interaction lengths. The scintillator consists of 3.6 m long and 18.3 cm wide strips. The 11 strips that are directly behind one another are ganged together through adiabatic light guides, one at each end, leading to 5" phototubes. This provides a single longitudinal sampling. Eighteen such assemblies are stacked vertically. The vertical coordinate of a hadron is obtained from the assembly number it is observed in and the horizontal coordinate by the ratio of the pulse height observed in the two phototubes at the two ends of the assembly. The energy resolution is $(100/\sqrt{E})\%$, with E in GeV, sufficient for the purpose of this experiment.

6 Further improvements

The basic design of the detector may be improved with techniques which still need feasibility studies. These will be made in a PS test beam in September 1997 [53].

We will describe in the following a number of the options which will be studied in the tests.

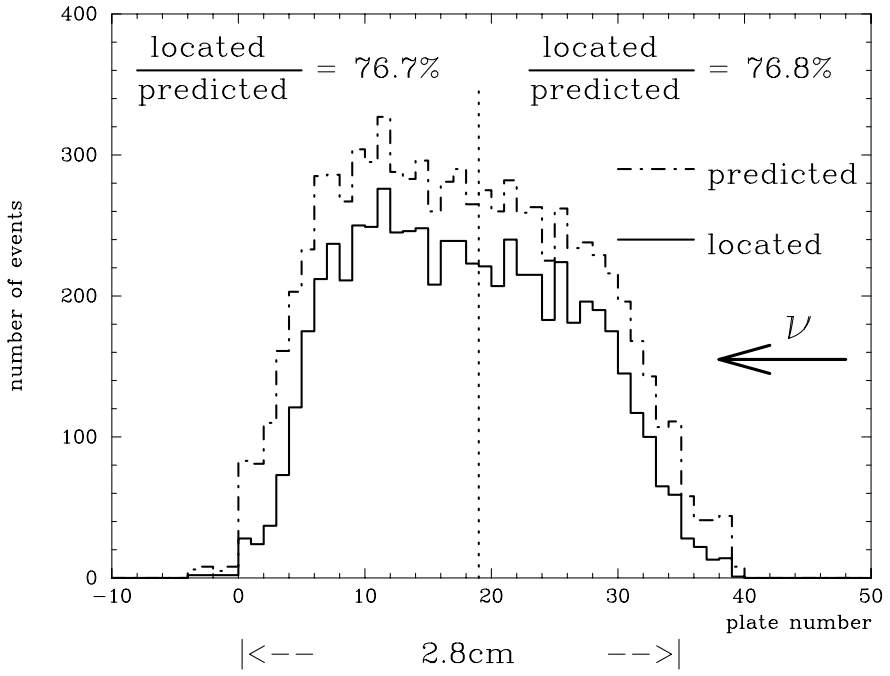

Figure 12: *The efficiency in CHORUS as a function of the predicted event vertex position. The reduction of events for larger depth into the target stack is attributed to event reconstruction losses. This interpretation is supported by the constant ratio of predicted and found events as function of the depth.*

6.1 A thicker target emulsion stack

In the CHORUS experiment, a small loss of events is visible in the upstream part of the target stack (Fig. 12). Since the ratio of found to predicted vertices remains constant over the stack, we conclude that this inefficiency can be assigned to pattern recognition difficulties in the electronic detectors. In the present design, this capability has been dramatically improved and one expects that this effect will be much weaker.

The scan-back efficiency in the target stack remains constant over the depth of the stack traversed. The possibility of using thicker target stacks, thus adding more mass while keeping the amount of electronic detectors constant, will therefore be tried out in the test beam.

6.2 Momentum measurement with separate emulsion plates

There exists a possibility to improve the momentum resolution by inserting special emulsion plates in the tracking section of each module. At the same time, the tracking section can then be made shorter, allowing for more target mass.

In the TENOR approach [34], each module is about 60 cm long. In this design, a module (Fig. 13) consists of:

- one target emulsion stack;

- a triplet of emulsion plates;

one emulsion plate, similar to those previously described, is placed just behind the target emulsion stack, a second one is located immediately in front of the following target emulsion stack, and a third is placed halfway between the first two outer plates. The middle plate determines a high precision space segment; this information, combined with that from the other two plates, allows momentum analysis by means of a sagitta measurement in the gap between consecutive stacks. The first plate also has the additional task of precisely locating the track in the target emulsion.

- a pair of silicon detector planes placed behind the first plate, to improve the track location in this emulsion sheet;

- electronic trackers consisting of honeycomb chambers each about 4 cm thick and measuring one of the x,y or inclined (u,v) coordinates.

With the angular measurement in the two outer plates alone one can estimate a momentum resolution:

$$(\Delta p/p)_{meas} = 0.9\% \times p[GeV/c]$$

in addition to a 2% contribution from the multiple scattering in the emulsion plates and in the electronic trackers.

The use of all information (angle and position) in all three plates improves the resolution. The relative alignment of the plates is performed using high-energy halo muons, and the alignment methods (and their requirements) have to be studied carefully. Assuming a precision (5 μm) about a factor five worse than the intrinsic resolution of the emulsion, and given the 51 cm total distance, we obtain a momentum resolution:

$$(\Delta p/p)_{meas} = 0.08\% \times p[GeV/c].$$

The total contribution of the Coulomb scattering to the momentum resolution amounts to about:

$$(\Delta p/p)_{MS} = 2.5\%,$$

by combining quadratically the position measurement and the multiple scattering contributions. In the momentum range of interest, the Coulomb scattering is such that the resolution does not depend critically on the assumed measurement errors. Even in the conservative case of a 20 μm precision, the total momentum resolution stays below 10% up to 30 GeV/c. The requirements on the relative plate alignment and on the spatial resolution thus appear to be within the experimental capabilities.

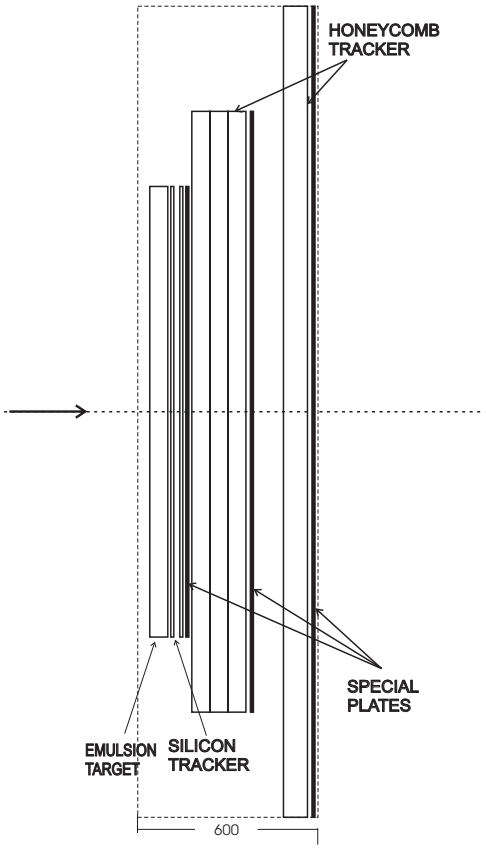

Figure 13: *The layout of a target module in TENOR.*

6.3 Momentum measurement in an extended target stack

Another method to perform momentum measurement with emulsion plates is to extend the target stack in the downstream direction with a set of special plates. These plates are mounted in three doublets, as shown in Fig. 14. The plates within a doublet are separated by 10 mm. The spacing between the doublets is 50 mm. This configuration allows for a crude momentum measurement of charged particles, with a very large acceptance, even without using the electronic detectors. This geometry can increase the acceptance in particular for large angle tracks.

6.3.1 Scan back strategy

The track segment defined by the silicon detectors is extrapolated onto the downstream plate of the last doublet. The prediction resolution is ~ 20 μm in the non-bending plane and for unknown momentum larger in the bending plane. The deviation due to magnetic deflection increases the scanning area to an extent which is acceptable in terms of scanning time.

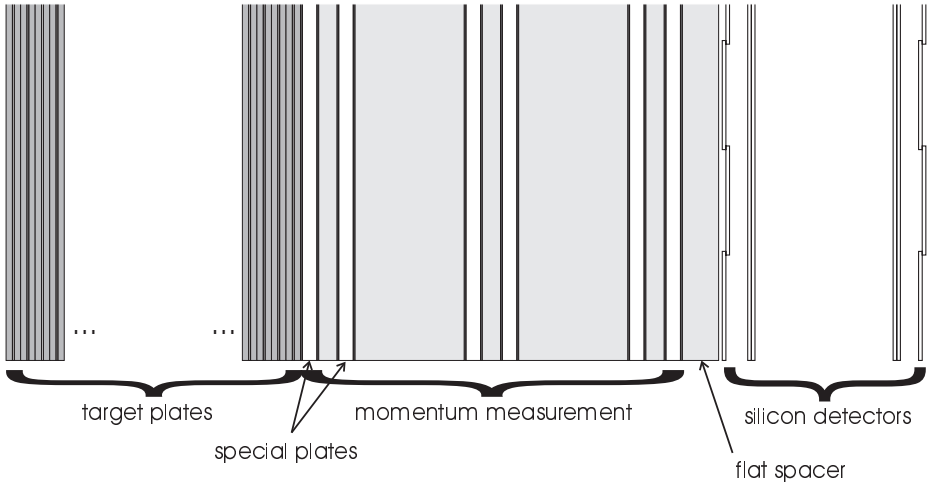

Figure 14: *Compact geometry for momentum measurement with emulsion plates.*

The knowledge of the impact point on the first special plate improves the precision of the prediction on the upstream member of the doublet. This allows an efficient search of the impact point on the upstream plate of the doublet.

The combination of the two points measured in the silicon detectors and the two points in the special emulsion plates gives already a sufficient estimate of the particle momentum to restrict the search area on the middle doublet. The points on the second doublet in turn improve the momentum resolution, thus allowing for a better precision on the most upstream doublet. The combination of the three doublets gives a resolution better than 10% for all tracks below 15 GeV/c, which can be further improved with the additional information from the silicon trackers and the wire chambers.

All tracks, which are found at the interaction point can be followed downstream to the three doublets, and can have their momentum measured. This is a very important feature for the kinemetical analysis of the events. It is expected that this system allows for high efficiency in the momentum reconstruction and makes it possible to install fewer or less performant wire chambers.

7 Sensitivity and background

The sensitivity to the ν_τ oscillation signal and the background estimation are shown separately for the following single charged particle decay modes of τ:

$$\tau^- \to \mu^- \nu_\tau \overline{\nu}_\mu,$$

$$\tau^- \to e^- \nu_\tau \overline{\nu}_e,$$

$$\tau^- \to h^- \nu_\tau (n\pi^0).$$

Charged current interactions of ν_τ can be selected on the basis of their characteristic topology in 1-prong decay channels. The basic selection is a decay vertex at a distance greater than 20 μm

and less than 3.5 mm from the neutrino interaction vertex, one negatively charged track from this secondary vertex that gives rise to a kink angle greater that 10 $mrad$ and no identified muon or electron at the primary vertex.

The three-prong decay $\tau^- \rightarrow \pi^+\pi^-\pi^-(n\pi^0)$, with a branching ratio of about 14%, can further improve the efficiency of τ detection. Efficiency and background studies are under way in order to estimate the additional contribution to the sensitivity.

The decays of π^- and K^- produced in NC and CC neutrino interactions can simulate the 1-prong topology. They can be easily removed by requiring the transverse momentum of the candidate's charged daughter relative to the parent direction, p^T_{decay}, to be greater than 250 MeV/c. After this cut the remaining background sources are:

1. the prompt ν_τ contamination in the beam;
2. one-prong decays of *charm* antiparticles;
3. hadrons that scatter in the emulsion with no visible additional activity, the so-called *white kinks*.

A preselection, needed to reconstruct the event and determine the charge of the decay daughter, and kink detection cuts affect in a different way both signal and background as is shown in Tab. 2, 3, 4, 5, 6, 7.

In order to enhance the signal to noise ratio, kinematical analysis at the primary and decay vertices, which exploit both the space resolution of the emulsion and the full spectrometry of the event, are exploited. These reduce the background from charm and white kinks. This analysis needs only to be performed for candidate events.

Prompt ν_τ interactions and the oscillation signal have different energy spectra, as can be seen in Fig. 15, where the candidate spectrum is approximated by the ν_μ spectrum [1]. The difference between the spectra is more significant at low Δm^2, as the ν_τ from oscillation becomes softer, thus allowing a more powerful discrimination. In the following all efficiencies will be computed in the hypothesis of large Δm^2.

7.1 Muon decay channel

The search for τ decays into muon takes advantage of a clear topology and a low background. Preliminary results have been presented [54] by the CHORUS experiment and they allow to estimate the expected efficiency of the proposed experiment on an experimental basis, as shown in Tab. 2.

The increase of the sensitivity, by a factor close to 3 compared to CHORUS, is achieved by:

- higher kink finding efficiency, obtained by:
  - better tracking, so that the muon assignment is unambiguous;
  - analysis of the "video image" at the vertex for kink finding;
  - higher resolution on p^T_{decay};
  - reduction of decays outside the stack by a factor 2 owing to the increased stack thickness;

[1] This corresponds to a two neutrino mixing scheme in the limit of oscillation with $\Delta m^2 \rightarrow \infty$

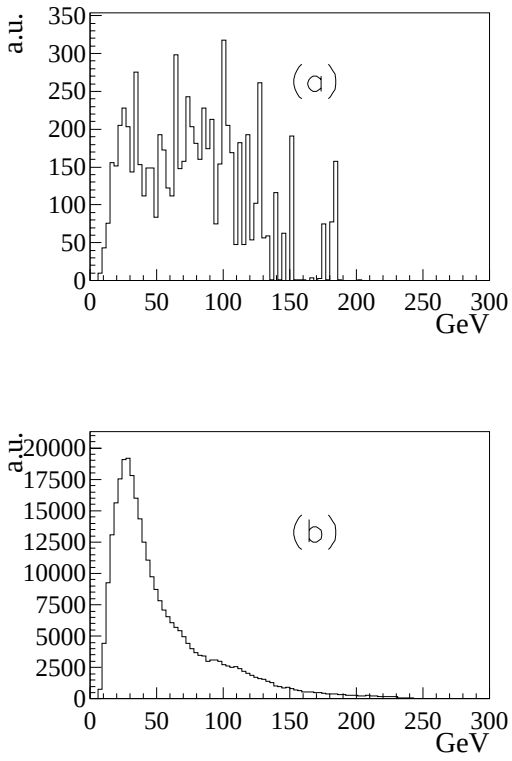

Figure 15: *Energy spectra for interacting neutrinos: (a) ν_τ prompt; (b) ν_τ from oscillation ($\Delta m^2 > 10^3\, eV^2$).*

- higher scanning efficiency, mainly achieved by:
  - larger relative fiducial volume, 95% (80% in CHORUS);
  - smaller losses at the emulsion interface due to precision external detectors, 10% (30% CHORUS). It should be noted that the silicon-emulsion track finding inside a magnetic field will be studied in a test beam;
  - higher target scanning efficiency, 90% (84% in CHORUS);
- detectors with better time response, improving pattern recognition by reduction of overlay hits and decreasing dead time.

For the muon decay mode the main background channel is given by single charm production in antineutrino CC interactions:

$$\bar{\nu}_\mu N \rightarrow \quad D^- \mu^+ X$$

$$\bar{\nu}_e N \rightarrow \quad D^- e^+ X$$

when the D^- decays into a negative muon and neutral particles.

Selection	$\tau^- \to \mu^-$	CHORUS
μ^- reconstructed	0.90	0.65
$p_\mu < 30\ GeV$	0.89	0.89
kink finding	0.75	0.61
scanning	0.75	0.45
detector (trigger and dead time)	0.94	0.90
Detection efficiency	0.42	0.14
$\sigma_{\nu_\tau}/\sigma_{\nu_\mu}$	0.50	0.53
B.R.	0.18	0.18
Sensitivity	0.037	0.014

Table 2: *Sensitivity to* $\tau \to \mu^- \bar{\nu}_\mu \nu_\tau$.

	$\bar{\nu}_\mu$ (1)	$\bar{\nu}_e$ (2)	ν_τ (3)
Flux $\times$ cross section	$2.0 \cdot 10^{-4}$	$1.0 \cdot 10^{-5}$	$1.1 \cdot 10^{-6}$
B.R. ($D^- \to \mu^-$ + neutrals)	0.10	0.10	0.178
μ^- reconstruction	0.90	0.90	0.90
missing primary lepton	0.026	0.10	-
$p_\mu < 30\ GeV$	0.99	0.99	0.80
kink efficiency	0.53	0.53	0.72
scanning efficiency	0.75	0.75	0.75
detector efficiency	0.94	0.94	0.94
Background rate (10^{-7}) / N_{CC}	1.7	0.3	0.7

Table 3: *Main sources of background for the muon decay channel normalized to the number of CC events.*

The calculation of the ratio of background events over the number of ν_μ charged current interactions is given in Tab. 3, where the last column represents the prompt ν_τ contribution.

The associated $c\bar{c}$ production in neutral and charged currents ν_μ interactions can be neglected because the cross-section is small and the background can be suppressed by the detection of the second decay vertex and through kinematical analysis. Kinematical cuts are very selective for the NC case due to the p^T of the primary neutrino.

7.2 Electron decay channel

The momentum and charge of electrons from τ decay may be determined by the bending in the magnetic field if they do not induce heavy showers in the emulsion. An electron is identified with high efficiency in the emulsion by looking at e^+e^- pairs produced along the trajectory by the conversion of bremsstrahlung γ's or by electromagnetic calorimetry.

Here it is assumed that 90% of the electrons that can be followed outside the stack are identified. Therefore the candidate search can be done using the guidelines of the muon channel. The selection efficiencies are summarised in Tab. 4. The background estimates (Tab. 5) are obtained by just rescaling the one for the muon decay mode by the ratio of sensitivities.

Selection	$\tau^- \to e^-$
e^- tracking and id	0.22
$p_e < 30\ GeV$	0.89
kink finding	0.75
scanning	0.75
detector (trigger and dead time)	0.94
Detection efficiency	0.106
$\sigma_{\nu_\tau}/\sigma_{\nu_\mu}$	0.50
B.R.	0.178
Sensitivity	0.009

Table 4: *Sensitivity to* $\tau \to e^- \bar{\nu}_e \nu_\tau$

	$\bar{\nu}_\mu$ (1)	$\bar{\nu}_e$ (2)	ν_τ (3)
Background rate $(10^{-7})/\ N_{CC}$	0.42	0.07	0.17

Table 5: *Main sources of background for the electron decay channel.*

7.3 Single hadron decay channel

These are selected among the events with no detected muon or electron daughter. It is required that the hadron is negative and that its measured momentum is between 2.5 and 30 GeV/c. These limits are justified by the improvement of the signal to noise ratio. The white kink background is important at low momentum (and small kink angles). For this reason a slightly harder cut on the transverse momentum of the decay is required here ($p^T_{decay} > 300\ MeV/c$). The final sensitivity is again higher by a factor 3 over that expected in CHORUS [20], as seen in Tab. 6.

The charm and prompt contribution to background are shown in Tab. 7. However, in this case, the main source are the white kinks and the A_1 coherent production. The background from white kinks depends on the number of negative charged tracks at the primary vertex ($\bar{n}_{h^-}$) in the sample

Selection	$\tau \to h^-$
h^- reconstructed	0.90
$2.5\ GeV < p_h < 30\ GeV$	0.69
kink finding (p^T_{decay} >0.3 GeV)	0.62
scanning	0.75
detector (trigger and dead time)	0.94
Detection efficiency	0.27
$\sigma_{\nu_\tau}/\sigma_{\nu_\mu}$	0.50
B.R.	0.50
Sensitivity	0.068

Table 6: *Sensitivity to* $\tau \to h^-(n\pi^0)\nu_\tau$.

	$\bar{\nu}_\mu$ (1)	$\bar{\nu}_e$ (2)	ν_τ (3)
Flux × cross section	$2.0 \cdot 10^{-4}$	$1.0 \cdot 10^{-5}$	$1.1 \cdot 10^{-6}$
B.R. ($D^- \to h^-$ + neutrals)	0.24	0.24	0.50
h^- reconstruction	0.90	0.90	0.90
missing primary lepton	0.026	0.10	-
2.5 $GeV < p_h <$ 30 GeV	0.71	0.71	0.54
kink efficiency	0.43	0.43	0.57
scanning efficiency	0.75	0.75	0.75
detector efficiency	0.94	0.94	0.94
Background rate (10^{-7}) / N_{CC}	2.4	0.4	1.1

Table 7: *Charm and prompt ν_τ background in the hadron decay channel.*

of events selected for scanning, on the scanning length l_{scan} and on the cross-section. A mean free path of λ_{WK}= 370 m for $p^T > 300$ MeV/c, as measured by a dedicated experiment with 4 GeV/c pions [55], has been used in this calculation. It is also assumed that the measured exponential p^T fall-off is independent of the pion kinematics. These assumptions can be checked by the new measurements at lower momentum expected to be available soon. Within the envisaged experiment itself, results can be obtained by relaxing selection criteria.

Thus the white kink contribution is given by:

$$\begin{aligned} N_{WK} &= \frac{NC}{CC}\ \bar{n}_{h^-}\ \frac{l_{scan}}{\lambda_{WK}}\ \epsilon_{rec.}\ \epsilon_{kin.}\ \epsilon_{scan.}\ \epsilon_{det.}\ N_{CC} \\ &= 0.3 \cdot 1.5 \cdot \frac{3.5 \cdot 10^{-3}}{3.7 \times 10^2} \cdot 0.9 \cdot 0.34 \cdot 0.75 \cdot 0.94 \cdot N_{CC} \\ &= 9.2 \times 10^{-7} N_{CC} \end{aligned}$$

The coherent A_1 production has not been modelled. It was estimated within the CHORUS experiment[2] and its effect turns out to be similar to the one of the white kink ($\frac{A_1}{WK} = 1.18$).

7.4 Background rejection

Both A_1 and white kink background from neutral current events can be suppressed by kinematical analysis. The white kink events were studied in detail. In the plane perpendicular to the beam, the direction of the hadron shower is back to back to the τ candidate (CC interaction), but not to the pion kink parent, due to the missing neutrino (NC interaction). The distribution of the angle $\phi_{shower-kink}$ for signal and background are shown in Fig. 16.

It should be noted that, since NC do not probe the u/d valence quark composition in the same way CC do, there is another observable difference between CC and NC interactions: the ratio between the number of events with an odd number of charged tracks and an even number. For emulsion Z/A is about 0.45, therefore the expected ratios are 1:3 and 1:1 respectively. Applying a harder cut on $\phi_{kink-sh}$ on the odd sample, a rejection factor 23 with a τ detection efficiency of 70% can be obtained. Since this rejection criteria are not based on the decay properties of the candidate (kink angle, daughter momentum, decay length), similar results are expected for the A_1 background.

In Tab. 8 the number of expected background events has been computed taking into account cuts that yield a factor of 15 reduction of the charm sources while retaining 70% of the signal. The charm

[2] in the kinematical region, $1 < p_h < 15$ GeV

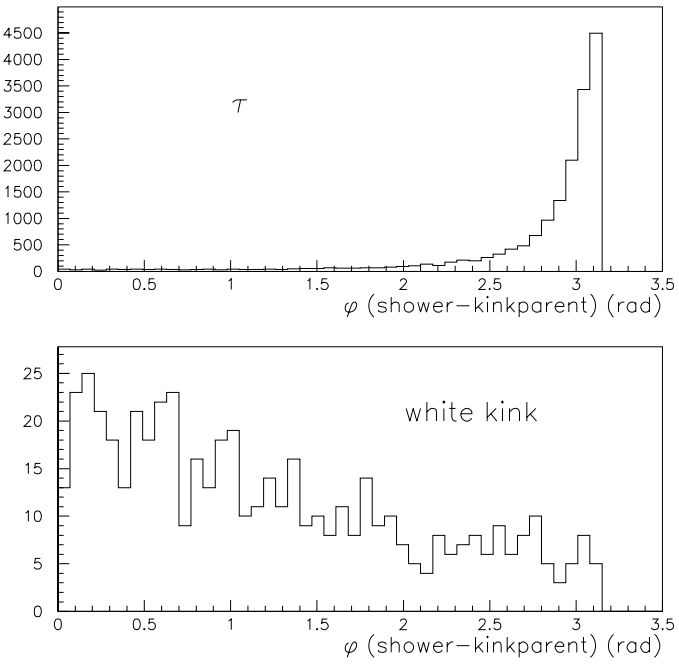

Figure 16: *Signal and background distributions of the angle between the shower direction and the candidate in the transverse plane.*

suppression can be achieved by a selection on Q^T, the transverse momentum of the shower w.r.t. the kink parent and the angle of the candidate w.r.t. the beam. The two-dimensional scatter plots of these variables are shown in figure 17.

The cuts that have been studied for the charm rejection suppress further the white kink and viceversa. In the computation of the sensitivity to $\tau \rightarrow h^-(n\pi^0)$, the correlation between the two sets has been taken into account for the white kink, which will be reduced by a factor 30 by all selection criteria at the vertex. These criteria result in a 55% signal reduction. To evaluate the possible effect on the charm, higher statistics would be needed. For this reason the charm contributions to background shown in the Table have to be taken as upper limits. It has to be noted that the vertex cuts suppress the prompt ν_τ and the signal by a similar amount.

7.5 Expected sensitivity

The experiment is left with 1.3 background events for a total number of 6×10^6 charged current interaction induced by ν_μ. If 1 event is really observed this implies a 90% C.L. upper limit of 3.2 τ^- events. The corresponding oscillation probability is 0.75×10^{-5}. The limit in the mixing angle, for large Δm^2, is:

$$sin^2 2\theta \ < \ 1.5 \times 10^{-5}$$

For full mixing, the minimum detectable Δm^2 at 90% C.L. is 0.1 eV^2.

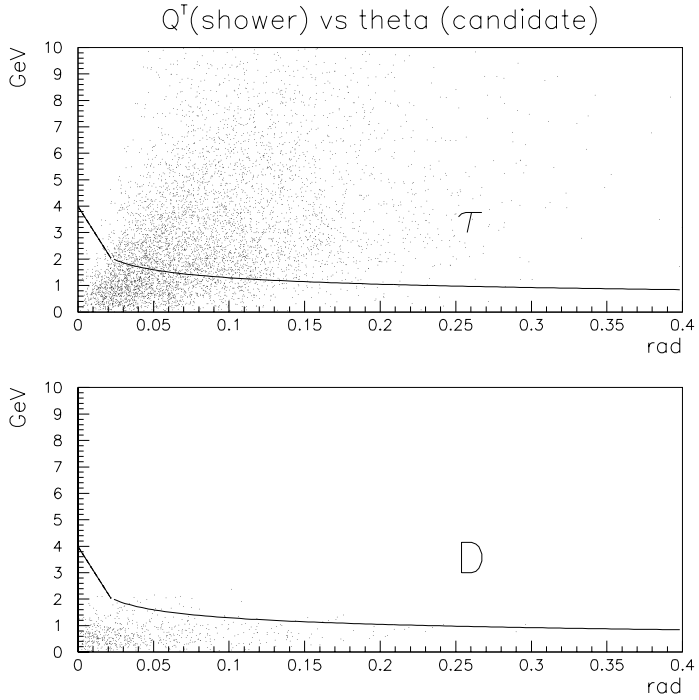

Figure 17: *Signal and background distribution of Q^T vs the angle of the candidate w.r.t. the beam direction.*

Decay mode	Oscillation sensitivity	background channel	events for 6×10^6 ν_μCC
μ	0.026		
		$\overline{\nu}_\mu$ charm	0.07
		$\overline{\nu}_e$ charm	0.01
		ν_τ prompt	0.29
e	0.006		
		$\overline{\nu}_\mu$ charm	0.02
		$\overline{\nu}_e$ charm	0.00
		ν_τ prompt	0.07
$h^-(\mathrm{n}\pi^0)$	0.038		
		$\overline{\nu}_\mu$ charm	0.09
		$\overline{\nu}_e$ charm	0.02
		ν_τ prompt	0.36
		white kink + A_1	0.38
Total			
		charm	0.2
		ν_τ prompt	0.7
		white kink + A_1	0.4
	0.070		1.3

Table 8: *Summary of efficiencies and backgrounds after kinematical analysis.*

The exclusion plot in the plane $\Delta\, m^2$-$sin^2 2\theta$ is given in Fig. 18. The curve bounds the areas that are excluded at 90% C.L. if no oscillation signal over the expected background is found. The expected sensitivity of CHORUS and NOMAD after a 4 years run (1994–1997) is also shown, as well as the present best limit.

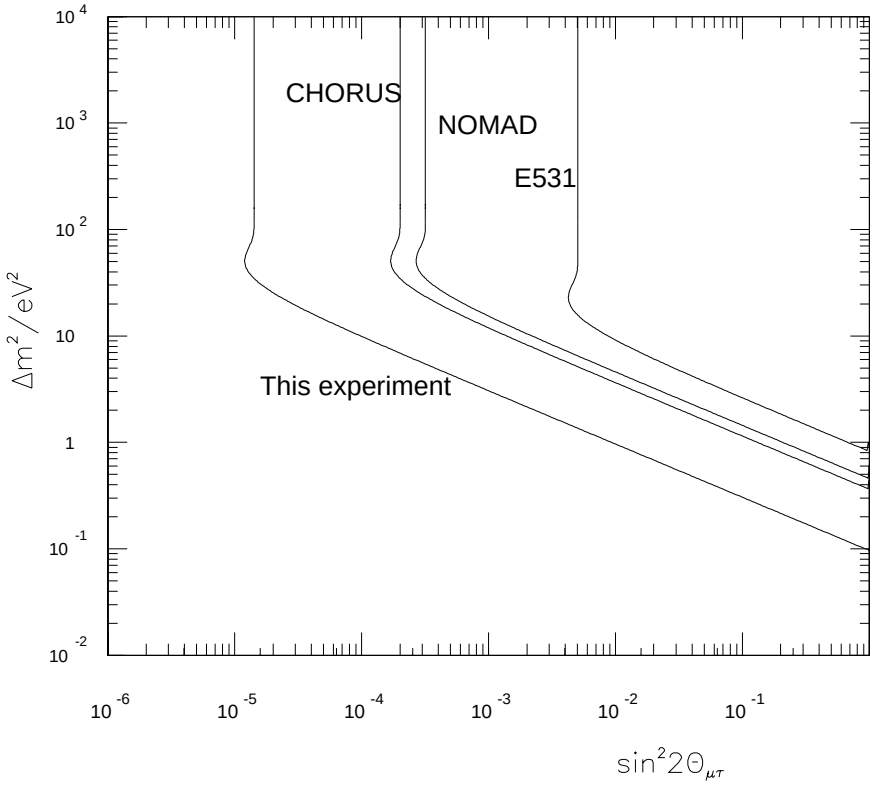

Figure 18: *Exclusion plot (90% C.L.) in the plane* $\Delta\ m^2$-$sin^2 2\theta$.

In a scenario involving a small $\Delta m^2(10^{-2}\ eV^2)$ and a second large $\Delta m^2(1\ eV^2)$ [17] this experiment would observe about 20 events.

Given the 1% ν_e content of the beam, this experiment will also set a limit on $sin^2 2\theta\ \sim\ 10^{-3}$ on $\nu_e \leftrightarrow \nu_\tau$ oscillation for large $\Delta\ m^2$, with a minimum detectable $\Delta\ m^2\ \sim\ 1\ eV^2$ for full mixing.

8 Conclusions

In conclusion, we have shown that, building on the expertise being acquired in CHORUS, NOMAD and NOMAD-STAR, and on the ideas discussed within the neutrino community, the techniques of

emulsion and silicon can be combined into a powerful detector to search for $\nu_\mu \leftrightarrow \nu_\tau$ oscillation. The experiment will exploit the direct detection of the τ^- decay topology with an effective kinematical analysis of the candidate events.

Recent advances in fast automatic scanning techniques obviate the need for the preselection of events resulting in an improved efficiency for the detection of τ^-. This efficiency is improved further by the accurate extrapolation of tracks to the emulsion provided by the silicon tracker. The scanning of all events appears feasible in about two years from the end of the data taking.

A careful study of the CERN accelerator chain capabilities has shown that a gain of a factor of two in protons on target per second can be achieved by the existing SPS Wide Band Beam.

Taking all these factors together the detector described in this Letter of Intent could improve the limit to be set by CHORUS and NOMAD, if they do not observe any oscillation candidates, by a factor of twenty reaching a sensitivity of $sin^2(2\theta) \sim 1.5 \times 10^{-5}$ at high Δm^2 and $\Delta m^2 \sim 0.1\ eV^2$ at maximal mixing. Alternatively, if the present short base line experiments detect a few τ^- candidates this detector would observe about 100 events (with a background of only one event) which would allow a more detailed study of the oscillation parameters.

In a scenario involving a small Δm^2 ($10^{-2}\ eV^2$) and a second large Δm^2 ($1\ eV^2$) proposed recently to explain the LSND, solar and atmospheric results, this experiment would observe about 20 events with negligible background.

It should be pointed out that Cold-Hot Dark Matter scenarios greatly favour a ν_τ with a mass of a few eV. If such a neutrino resulted in a Δm^2 of $10\ eV^2$ then this experiment could detect it even if an oscillation strength as low as $sin^2(2\theta) \sim 10^{-4}$ prevailed.

We believe that the detector can be realized in three years. A technical run in the year 2001 can be envisaged, with data-taking in the years 2002–2004.

A Neutrino oscillation scenarios

A.1 First scenario: "Solar+LSND" or "Solar+Atmospheric"

In this scenario the "small" Δm^2 is constrained by the solar neutrino data, assuming matter-enhanced oscillations [56]. Then the "large" Δm^2 can be used to explain either the LSND results [57] or the atmospheric neutrino deficit [58], but not both (unless the Kamiokande atmospheric data in the multi-GeV range are dropped [59]).

If one takes the first option (Solar+LSND) and a mass spectrum with two light neutrinos (ν_1, ν_2), plus a heavy neutrino (ν_3) in the eV range, then the combined fit [56, 57] prefers a strong mixing of ν_3 with ν_μ, with (ν_1, ν_2) being essentially a mixture of (ν_e, ν_τ). High-sensitivity neutrino oscillation searches in the $\nu_\mu \leftrightarrow \nu_\tau$ channel are able to probe a fraction of the LSND signal [57].

The second option (Solar+Atmospheric) leads one to a larger variety of mass-mixing solutions [56, 58] which are in the range of interest for long-baseline experiments.

A.2 Second scenario: "Solar+Atmospheric"

The threefold maximal mixing scenario [60, 61] assumes a democratic (*i.e.* 1/3, 1/3, 1/3) flavour content for the neutrino mass eigenstates. The "large" Δm^2 is basically constrained by the atmospheric neutrino data in the range relevant for LBL experiments. The "small" Δm^2 is weakly constrained by solar neutrino data to be below 10^{-11} eV^2. The Homestake and Kamiokande data cannot be fit simultaneously in this scenario [62].

The LSND results (and, in general, any evidence of oscillations with Δm^2 in the eV^2 range) cannot be accommodated in this framework, which is anyway compatible with the other negative searches at accelerators and reactors [60, 62].

A.3 Third scenario: "Solar+Atmospheric+LSND"

In the scenario proposed in [63, 17] the "small" Δm^2 is used to fit the atmospheric neutrino data, while the "large" Δm^2 is used to explain the LSND data. Then the survival probability for solar neutrinos is predicted to be energy-independent. This is not in good agreement with solar neutrino data, even taking the ^8B neutrino flux as a free parameter [64]. In the approximation of averaged atmospheric neutrino oscillation, and stretching the data to their 90–95% C.L. limits, one can fit all the data with two Δm^2 in the range $\sim 10^{-2}$ and 1-2 eV^2, and with a specific mixing matrix [63].

References

[1] J. Primack et al., Phys. Rev. Lett. 74 (1995) 2160; S. Ghigna et al. astro-ph/9611103.

[2] B.T. Cleveland et al. (Homestake Collaboration) Nucl. Phys. B47 (1995); and talk given at XVII Int. Conf. on Neutrino Physics and Astrophysics, Helsinki, Finland, 13-19 June 1996.

[3] V.N. Gavrin, (SAGE Collaboration), talk given at XVII Int. Conf. on Neutrino Physics and Astrophysics, Helsinki, Finland, 13-19 June 1996; T. Kirsten (GALLEX Collaboration), talk given at XVII Int. Conf. on Neutrino Physics and Astrophysics, Helsinki, Finland, 13-19 June 1996.

[4] J.N. Bahcall and M. Pinsoneault, hep-ph/9610592.

[5] N. Hata and P. Langacker, Phys. Rev. D52 (1995) 420.

[6] Y. Fukuda et al., Phys. Lett. B 335, 237 (1994).

[7] S.P. Mikheyev and A. Yu. Smirnov, Yad. Fiz. 42 (1985) 1441; L. Wolfenstein, Phys. Rev. D17 (1985) 2369.

[8] L. Krauss, E. Gates and M. White, Phys. Lett. B299 (1993) 94; P.I. Krastev and S.T. Petcov Phys. Lett. B299 (1993) 99.

[9] C. Athanassopoulos et al., nucl.-ex9605003, (1996).

[10] J. Peltoniemi and J. W. F. Valle, Nucl. Phys. B406 (1993) 409.

[11] D.O. Caldwell and R.N. Mohapatra, Phys. Rev. D48 (1993) 3259.

[12] J.J. Gomez-Cadenas and M.C. Gonzales-Garcia, Z. Phys. C71 (1996) 443-454.

[13] J. Peltoniemi, D. Tommasini and J. W. F. Valle, Phys. Lett. B298 (1993) 383.

[14] G.L. Fogli, E. Lisi and D. Montanino, Phys. Rev. D49 (1994) 3626; CERN-TH/7491-94.

[15] J. Ellis, CERN-TH/96-325.

[16] P.F. Harrison, D.H. Perkins, W.G. Scott, Phys. Lett. B 349 137 (1995).

[17] A. Acker and S. Pakvasa, hep-ph/9611423 v2, 27 Nov. 1996.

[18] J. Primack hep-ph/9610321; J. Primack and A. Klypin astro-ph/9607061.

[19] H. Harari, Phys. Lett. B 216, 413 (1989).

[20] CHORUS Collaboration, M. de Jong et al., A new search for $\nu_\mu - \nu_\tau$ oscillation, CERN-PPE/93-131.

[21] NOMAD Collaboration, P. Astier et al., CERN-SPSLC/91-21 (1991), CERN SPSLC/9148, SPSLC/P261 Add.1.

[22] G. Ewan et al., Sudbury Neutrino Observatory Proposal, SNO-87-12 (1987).

[23] C. Arpesella et al., Borexino Proposal, vols 1 and 2, ed. G.Bellini and R. S. Raghavan, Univ. of Milan, (1991).

[24] H. de Kerret et al. The CHOOZ Experiment, LAPP Report (1993).

[25] J. Kleinfeller, (Karmen Collaboration), talk given at XVII Int. Conf. on Neutrino Physics and Astrophysics, Helsinki, Finland, 13-19 June 1996.

[26] N. Ushida et al., Phys. Lett. 206B (1988) 375.

[27] E. Ables et al., (MINOS Coll.), Fermilab Proposal P-875, (1995).

[28] COSMOS Collaboration, 1995 Update Report on Fermilab E803/COSMOS.

[29] ICARUS Proposal, LNGS-94/99-I (1994).

[30] M. Ambrosio et al., (NOE Collaboration), Nucl. Inst. Meth. A363 (1995) 604.

[31] T. Ypsilantis, Nucl. Instr. and Meth. A371 (1996) 330.

[32] ICARUS-CERN-Milano Coll., CERN/SPSLC 96-58, SPSLC/P 304 (1996).

[33] J.J. Gomez-Cadenas, J.A. Hernando and A. Bueno, Nucl. Instr. and Meth. A378 (1996) 196, and J.J. Gomez-Cadenas and J.A. Hernando, Nucl. Instr. and Meth. A381 (1996) 223-235.

[34] A. Ereditato, G. Romano and P. Strolin, INFN Napoli Int.Report, 16 February 1996, and A. Ereditato, G. Romano and P. Strolin, CERN-PPE/106-96, to be published in Nucl. Instr. and Meth.

[35] L. Ludovici and P. Zucchelli, CERN-PPE/96-181.

[36] CHORUS collaboration, CERN/SPSLC95-21,SPSLC/M543.

[37] S. Aoki et al., Nucl. Instr. and Meth. B 51, 446 (1990).

[38] T. Nakano, Ph.D. Thesis, University of Nagoya (1997).

[39] G. Rosa et al., Prep. Univ. Salerno DSF US 97/1 (1997), submitted to Nucl. Instr. and Meth..

[40] J.J. Gomez-Cadenas, "Design of a large area silicon tracker for a future neutrino oscillation experiment", inv. paper at the 6th VERTEX-96 Conference, Cagliari, June 1996. D. Ferrere, "Development of a silicon tracker for neutrino physics", presented at the 5th Int. Conf. on Advanced Technology and Particle Physics, Como, October 1996.

[41] WA17 Collaboration, Nucl. Phys. B 176 (1980) 13.

[42] E. Heijne, CERN Yellow Report, CERN 83-06, July 1983.

[43] G. Acquistapace *et al.* , CERN Internal Note, CERN-ECP 95-14, July 1995.

[44] L. Casagrande *et al.* , CERN Yellow Report, CERN 96-06, August 1996.

[45] H. Butler *et al.* , CERN Internal Note, CERN-ECP 93-22, November 1993.

[46] SPY Collaboration, G. Ambrosini *et al.* , CERN-SPSLC/96-01.

[47] B. Van de Vyver and P. Zucchelli, CERN Internal Note, CERN-PPE/96-113, August 1996.

[48] M. C. Gonzalez-Garcia and J. J. Gomez-Cadenas, Phys. Rev. D55 (1997) 1297-1306.

[49] COMPASS Coll., CERN/SPSLC 96-14, SPSC-P 297, 1996.

[50] B. Goddard *et al.* , CERN Internal Note, CERN-SL/96-73, December 1996.

[51] H. Van der Graaf et al., Nucl. Instr. and Meth., A307 (1991) 220.

[52] P.P. Allport et al., Nucl. Instr. and Meth., A310 (1991) 155.

[53] Request for a test of emulsion-silicon configurations for a neutrino experiment, CERN-SPC/97-4, SPSC/M596, 21 February 1997.

[54] CHORUS status report, SPSC, 1997.

[55] KEK measurement in P803 Fermilab proposal, appendix D.

[56] G.L. Fogli, E. Lisi, and D. Montanino, Phys. Rev. D 54, 2048 (1996).

[57] G.L. Fogli, E. Lisi, and G. Scioscia, hep-ph/9702298; see also Phys. Rev. D 52, 5334 (1995).

[58] G.L. Fogli, E. Lisi, D. Montanino, and G. Scioscia, hep-ph/9607251, to be published in Phys. Rev. D.

[59] C.Y. Cardall and G.M. Fuller, Phys. Rev. D 53, 4421 (1996).

[60] P.F. Harrison, D.H. Perkins, and W.G. Scott, Phys. Lett. B 349, 137 (1995).

[61] C. Giunti, C.W. Kim, and J.D. Kim, Phys. Lett. B 352, 357 (1995).

[62] P.F. Harrison, D.H. Perkins, and W.G. Scott, hep-ph/9702243.

[63] H. Minakata, Phys. Rev. D 52, 6630 (1995).

[64] P.I. Krastev and S.T. Petcov, hep-ph/9612243.